Studies on an Estuarine Beach:
Short- and Long-term Morphological Change of Marina Bay Beach in San Francisco Bay

By

MARIO F. M. ACCORDINO
THESIS

Submitted in partial satisfaction of the requirements for the degree of

MASTER OF SCIENCE

in

Civil and Environmental Engineering

in the

OFFICE OF GRADUATE STUDIES

of the

UNIVERSITY OF CALIFORNIA

DAVIS

Approved:

_____
Alexander L. Forrest, Chair

_____
John L. Largier

_____
Fabián Bombardelli

Committee in Charge

2023

ABSTRACT

Estuarine beaches are unique, critical landscapes that serve a variety ecological, social, and shoreline protection purposes. They differ from ocean beaches in several ways, including their form and governing hydrodynamic processes. In San Francisco Bay, the historically widespread estuarine beaches that protected landward tidal marshes have been largely eliminated. One constructed beach that borders a tidal marsh, Marina Bay Beach in Richmond, was studied to examine how the morphology of this beach responds to a range of wave conditions. This study is motivated by a broader understanding of estuarine beaches in S.F. Bay, as an increasing number of nature-based sea-level rise adaptation strategies are constructed on the shoreline.

Through a combination of methods, including topographic transects, grain size analysis, particle tracking, wave data collection, remote sensing, and historical data analysis, the evolution of Marina Bay Beach on an annual and event-based timescale is described. In agreement with established theory of low-energy beaches, Marina Bay Beach exhibits quiescent stability in planform with isolated periods of morphological change driven by storm events wherein high-energy waves associated with high landward winds are coupled with high tides. These morphological changes include the formation of washover fans and could be leading Marina Bay Beach to transgress faster than sediment supply can replenish displaced mass. This dynamic could potentially create a future scenario of a breached barrier and lack of wave protection for the backbarrier marsh and eventually the shoreline trail.

ACKNOWLEDGEMENTS

I am deeply indebted to John Largier for guiding me throughout this process, introducing me to the world of estuarine beaches, and lending an unwavering sense of calm persistence to this endeavor. I was fortunate enough to be guided by a group of helpful colleagues at Dr. Largier's Coastal Oceanography Group. Robin Roettger assisted with my field work and wave gage deployment. Will Speiser provided thoughtful suggestions and feedback regarding remote sensing technologies and methodologies, and Lukas WinklerPrins was instrumental in my wave data analysis efforts, both from a technical and conceptual perspective. Dr. Largier also introduced me to a team of experts in the field of estuarine shoreline research, design, and construction, including Roger Leventhal, Peter Baye, and Dan Gillenwater. I am grateful for their collaboration and guidance on this and other projects. In addition to Dr. Largier, the thesis committee of Drs. Alex Forrest and Fabian Bombardelli provided invaluable feedback to this paper as well as numerous courses of fluid mechanics and continuous tutoring throughout my time at UC Davis. Karen Barad, Jacqueline Thalberg, and other residents of the Marina Bay neighborhood provided not only valuable local knowledge of the beach and its history but are the leading forces of maintenance and care of the Beach on a daily basis. As always, I greatly appreciate the continued support and interest from my parents John Accordino and Anne-Marie McCartan throughout my academic career. Finally, I would like to thank my wife Maggie Azary for her continued patience and support with this project, and for her companionship on trips to beaches throughout San Francisco Bay over the last two years.

Table of Contents

I. INTRODUCTION

The combined loss of wetland area and imminent threat of sea level rise has spurred political action and caused a rethinking of the shoreline in San Francisco Bay ("S.F. Bay", "the Bay") (Baye et al., 2020, SFEI and SPUR, 2019). While widespread and effective in the short term for protecting landward conditions from waves, hard-edge shoreline edges such as seawalls and revetments have numerous drawbacks. They are often costly to build and maintain and are unable to adapt in response to rising sea levels (NOAA et al., 2015). They have a fraction or none of the ecological value that natural shorelines offer, and they can reflect wave energy, further scouring and eroding the sediment at their base. Lastly, they do not provide the same physical or recreational connection to the water's edge, undermining the Bay's cultural resources.

As a natural-based shoreline alternative, estuarine beaches are typically valued less than ocean beaches for recreation and infrastructural uses (Nordstrom, 1992). However, with growing awareness and understanding of the problems associated with hard-edge shorelines, nature-based alternatives that offer protection to tidal marshes are being tested and implemented throughout the Bay. Nourishment or beach creation projects exist in built or planned form at Aramburu Island, Eden's Landing, Pier 94, Heron's Head Park, and numerous other locations (WWR, 2010, SCAPE, 2020, SFBRA, 2020). Not all Bay beach nourishment projects have the same intention or understanding of natural processes: some are intended primarily for public access and recreation, with developed backshore conditions and periodic sediment

nourishment (EBRPD, 2013, BAWT, 2020, PWA, 2009). Properly engineered and constructed beaches offer an adaptable alternative to hard-edge shorelines while also providing ecological benefit as sea levels rise and marshes become more threatened by increased wave energy (Pilkey, 2011).

Now is a critical time to study beaches in San Francisco Bay in order to further understand their governing characteristics and to better inform future management of the estuarine edge. While a limited but growing body of knowledge of S.F. Bay beaches exists, the pace of shoreline adaptation and estuarine beach construction projects warrants deeper investigation. The proximity of S.F. Bay beaches also allowed the author to combine in situ and remote data collection methods, as is discussed later in Methodology. This thesis aims to add to the existing research in support of this objective.

First, this paper examines the governing characteristics relevant to estuarine beaches, including hydrodynamic, geomorphic, anthropogenic, and biologic elements. Due to the interaction among these numerous characteristics, an estuarine beach cannot be understood solely through the analysis of one method of data collection. By applying a variety of desktop and field techniques to study the numerous process variables governing estuarine beaches, this paper asserts that a coupled methodology of decadal and seasonal observations can reveal short- and long-term morphologic trends of Marina Bay Beach in San Francisco Bay. Due to its artificially embayed nature, as is described in following sections, this study expected to find trends of long-term stability in beach planform at the study site, punctuated by infrequent

events of storm-driven change, created by the combination of sustained, strong, shore-incident winds at high tide and resulting in visible change to the beach's backshore. Finally, results from this study are used to help contextualize potential evolution of this site and other Bay beaches in the future.

II. BACKGROUND

a. HISTORY AND FORMATION OF SAN FRANCISCO BAY BEACHES

i. Wetland and beach development in S.F. Bay

San Francisco Bay has experienced dramatic changes in sediment dynamics. At the end of the last glacial epoch approximately 15,000 years ago, rising sea levels shifted the California shoreline east. 6,000 years ago, when the rate of sea level rise slowed, marshes were able to form in the present Bay as salt-tolerant vegetation became established at the water's edge (Beagle et al., 2015, Atwater, 1979). Both ocean sources and fluvial sources carried suspended sediment that was deposited at the water's edge, building the substrate for these marshes to thrive, as well as coarser sediment that lined the shorelines in front of many marshes as beaches. Historical mapping and T-sheets, surveys conducted by the United States Coast Survey (USCS) in the 19th Century (Grossinger et al., 2005), show extensive stretches of beach present in the Bay upon the intensive European advancement into the region in the 1800s, especially on the eastern shore of the Central Bay, including a majority of the shoreline in present-day Alameda County, as shown in Figure 1.

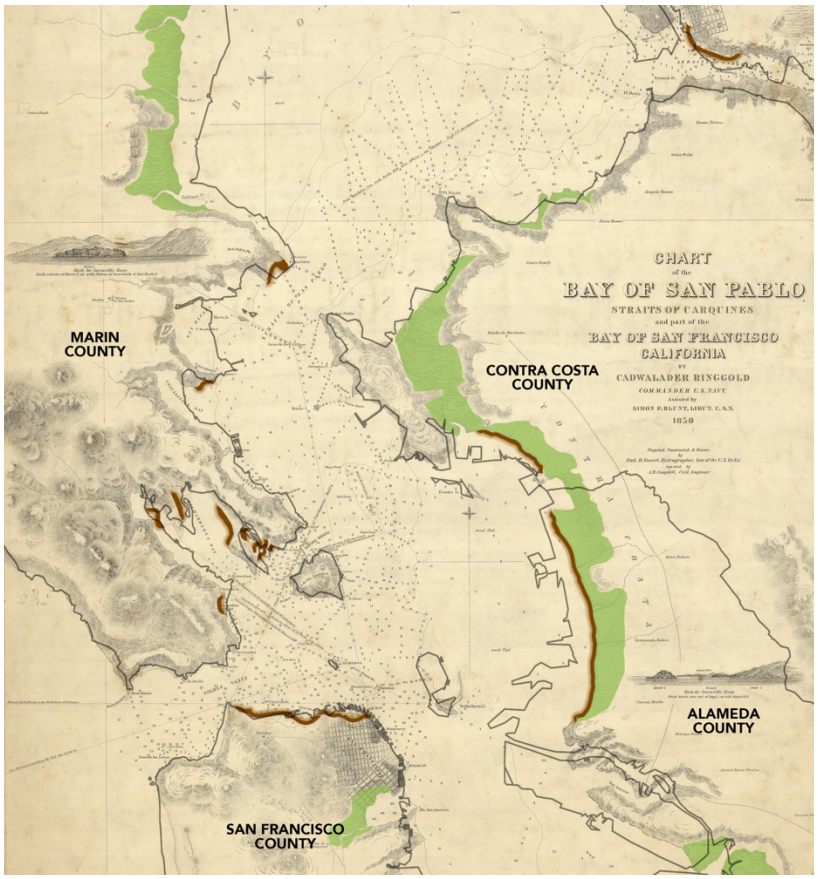

Figure 1. Central Bay Shoreline, 1853.

Significant historical beach systems highlighted in brown. Wetlands highlighted in green. Contemporary county borders labeled in black.

As described by SFEI and SPUR (2019), San Francisco Bay is surrounded by a heterogeneous geologic context and can be generally categorized into three 'geomorphic provinces' – rocky headlands primarily in the Central Bay, alluvial fans mostly within the Central East Bay, and alluvial plains in the North and South Bays. Rocky headlands provide bluff-sources of sediment for small pocket beaches embayed between erosion-resistant headlands, alluvial fans deposit coarse sediment through creek mouths which historically formed barriers in front of bay marshes, and alluvial plains are typically too gentle-sloping and wide for coarse sediment to be

carried to the Bay shoreline. These northern and southern-most sub-basins of alluvial plains within the Bay were, and remain, shallower and more turbid than the Central Bay.

In the second half of the 19th Century, hydraulic mining flushed large amounts of sediment through the San Joaquin – Sacramento Delta and into the Bay. Concurrently, wetlands throughout the Bay-Delta area were diked, drained and lined with levees for agricultural purposes. The 20th Century saw the continued acceleration of development on the water's edge, extensive channelization of creeks and the lining of the shoreline with levees, riprap revetments, seawalls, and other hard-edge infrastructure (SFEI and Baye, 2020). These conditions have separated marshes and beaches from their natural sources of sediment. As Schoelhammer (2011) identifies, the Bay has experienced a 'step change' in sediment supply, as the erodible storage of hydraulic debris-originated sediment supplying marsh development has been exhausted. As sea levels are projected to rise between 2.5 and 7.1 feet by 2100 (Petek, 2020), beaches and marshes throughout the Bay will struggle to maintain appropriate elevations for survival without a sediment source. Currently, only 5% of the area of pre-development wetlands still exists within the Bay (USGS, 1994). And as wetlands have become depleted, so have the beaches with which they existed.

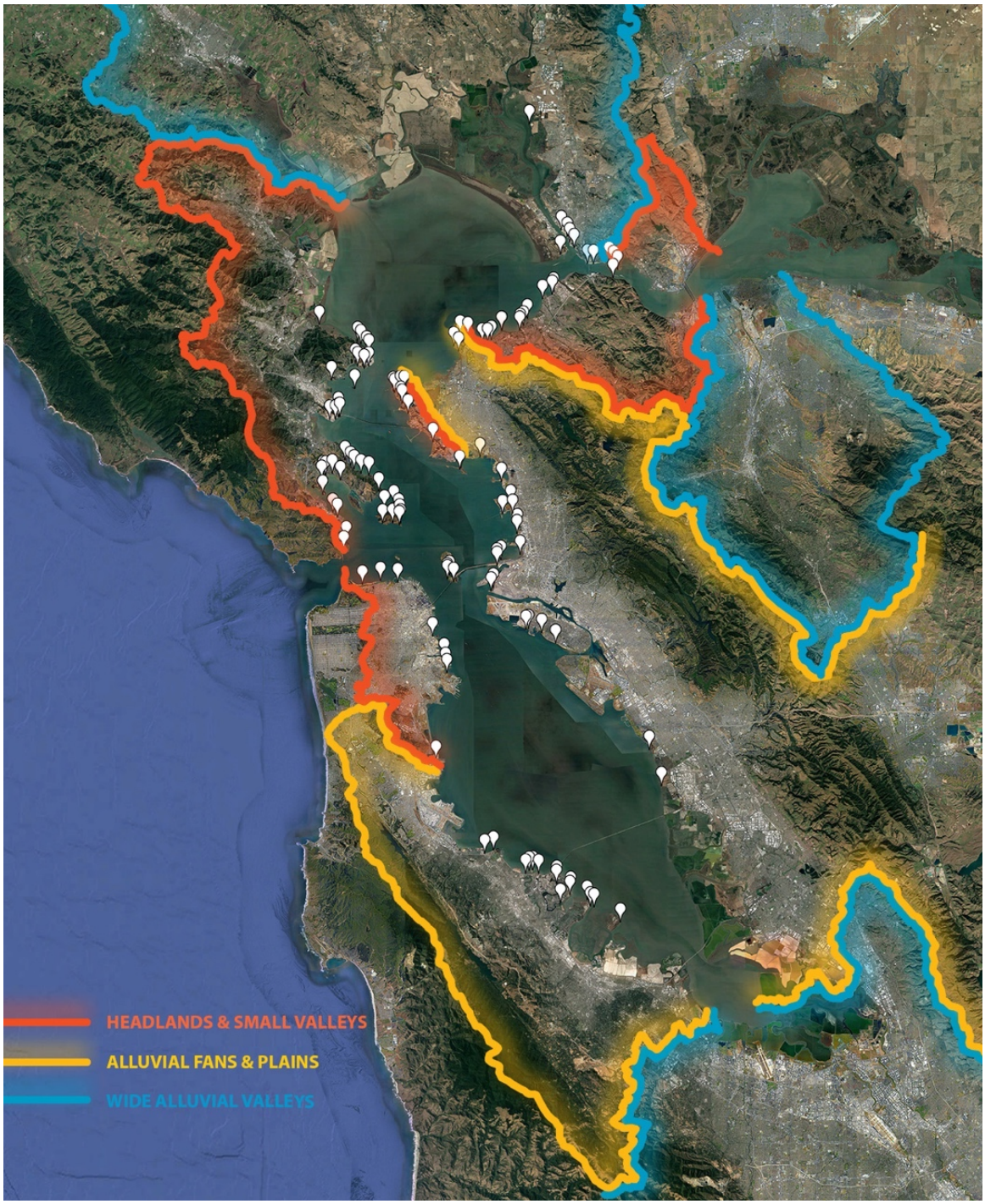

Figure 2. Spatial inventory of distinct San Francisco Bay beaches with geomorphic provinces, adapted from SFEI and SPUR, 2019. White dots represent beaches. List of beaches found in Table A1 in Appendix A.

From an analysis of aerial imagery, over one hundred distinct beaches currently exist in San Francisco Bay, as is seen in Figure 2 and listed in Table A1, Appendix A. The vast majority of these remaining beaches exist in the North-Central and South-Central Bay, within Contra Costa, Marin and Alameda Counties.

ii. Marsh erosion in S.F. Bay

While wetlands throughout the Bay were directly altered, many others have suffered indirectly as their sediment supply has dwindled. While marshes can drown if their elevation does not keep pace with sea level rise, they can also erode laterally, which is the primary mechanism for marsh erosion globally (SFEI and SPUR, 2019). San Pablo Bay has suffered from lateral marsh erosion between 2010-2018, with 27% of marshes experiencing erosion, as opposed to only 8% in the previous two decades (SFEI 2020, Beagle et al., 2015). As marsh edges are eroded by wave action, their wave-cut scarps serve as a vertical barrier that can reflect wave energy, resulting in scouring of the fronting mudflat or low marsh system. It is possible for beaches to form this way, as coarse sediment, if present in the marsh substrate, is removed and deposited at the water's edge (Nordstrom, 2022). However, the fine-grained fraction of this eroded sediment is likely to be carried away by tides (SFEI and Baye, 2020). The lower-intertidal erosion caused by reflected waves can result in an increased water depth in front of the marsh, which reduces wave attenuation effects. Future conditions will result in even deeper waters fronting marshes if low marshes and mudflats do not rise at the same rate as sea levels (Crosby

et al., 2016). In this context, estuarine beaches offer valuable lateral protection for these marsh edges in natural or constructed contexts (Nordstrom, 1992).

b. GOVERNING CHARACTERISTICS OF ESTUARINE BEACHES

Beaches in San Francisco Bay can be described by elements used globally to characterize both estuarine and ocean beaches, including geomorphic, hydrodynamic, and other factors.

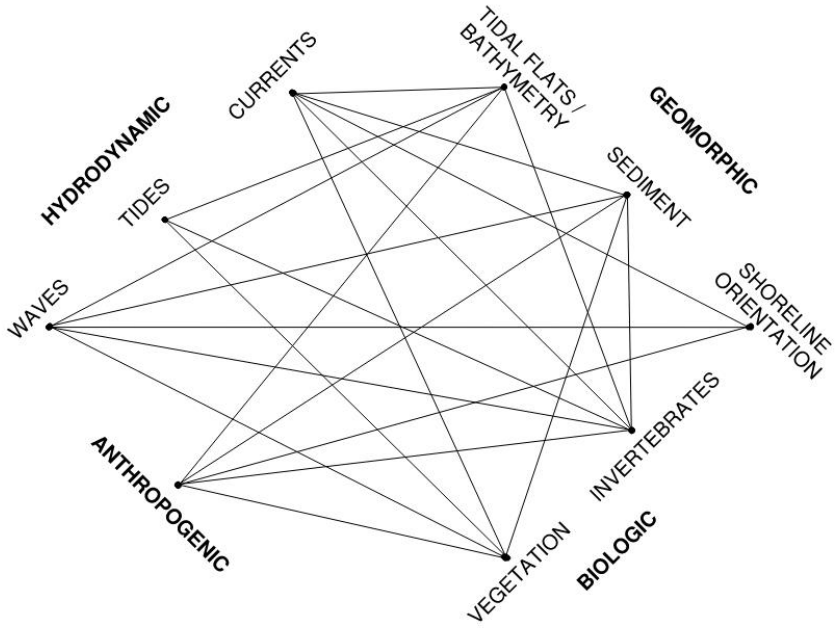

Figure 3. Primary governing characteristics of estuarine beaches. Lines represent interrelationships between characteristics.

While predominantly shorter and narrower, estuarine beaches are distinct from ocean beaches in several regards and are not simply 'scaled-down' versions of their high-energy counterparts (Nordstrom, 1992). A variety of terminology exists to distinguish beaches not located on a high-energy ocean shoreline. "Low-energy beaches" refers broadly to beaches that are

affected by waves of a certain height and energy. As defined by Jackson et al. (2002), non-storm significant wave heights reaching low-energy beaches are generally less than 0.82 ft (0.25 m), and storm waves are typically less than 1.64 ft (0.5 m). "Fetch-limited" beaches refer to beaches where the wave generation is dominated by wind waves, and the strength of waves reaching the beach is determined chiefly by the length of water over which the wind blows, or the fetch. This excludes low-energy sheltered beaches located in the lee of islands but can include beaches formed within lakes or reservoirs (Nordstrom and Jackson, 2012). "Beaches in estuaries and bays," or BEBs (Vila-Concejo et al., 2020), as well as the term estuarine beaches, refers to beaches that are located within these specific geographic contexts. While the terms estuary and bay are themselves often debated and can include high-energy ocean settings such as Monterey Bay in California, this term generally implies low-energy beaches located within estuaries and semi-enclosed bays, like San Francisco Bay.

Wind duration, speed, angle, fetch, shoreline orientation, tidal range, nearshore bathymetry, and sediment composition are the primary variables that influence an estuarine beach's morphology. The effects of these variables often compound or conflict each other, producing a wide range of beach forms. Heterogeneity in conditions along the estuarine shoreline often result in beaches that are more formally variable than those found on ocean coasts. These characteristics can vary within a short distance and can build composite, complex features within a single beach site.

i. Wave climate

Chief among differences between ocean and estuarine beaches is the associated wave period. Although varying proportions of wave periods may be present at an estuarine beach, they are most often sheltered from long-period, ocean-generated swell waves. These waves break or are dissipated by shallower water depths or shoreline topography as they propagate into a bay. Further away from the ocean entrance to an estuary or bay, estuarine beaches receive the dominant portion of their wave energy from short-period, locally generated wind waves (Nordstrom and Jackson, 2011). This results in waves that are generally less powerful than those acting on ocean beaches and implies a seasonal variability to the wave climate. That is, wave action is typically highest during seasons associated with strong winds although it is acknowledged that episodic wind events can occur at any point during the year (Nordstrom, 1980). However, waves that reach an estuarine beach can be a composite of ocean swell and locally generated wind waves. As examined by WinklerPrins et al. (2021), beaches in Tomales Bay display a gradient of wave sources; sites closer to the ocean exhibit longer-period, infragravity waves, sites located near the mouth of the estuary contain an approximately equal mix of infragravity, swell and wind chop waves, and sites near the head of the estuary are dominated by wind chop waves. Rahbani et al. (2022) found similarly varied wave signatures throughout BEBs in Australia's Botany Bay, where beaches further from the bay's entrance alternated between periods of primarily swell- and wind-wave influence. Notably, this gradient of wave signatures was spatially variable and influenced by anthropogenic interventions.

In San Francisco Bay, the beach at Crissy Field, at the mouth of the estuary, is impacted both by swell and wind waves (Battalio, 2014). For wind waves generated within a basin such as S.F. Bay, wave energy typically increases with the fetch. However, across short fetch and shallow water, waves will not increase in height even with increasing wind speed (Jackson et al, 2002). For example, although waves can blow over long distances in the North or South Bay, this water is generally shallow in these sub-basins, so waves reaching these shorelines generally contain less energy than in the Central Bay.

In addition to swell and wind waves, boat wakes can create morphologically influential waves in estuaries and bays (Nordstrom, 1992). While not presently a major source of waves in S.F. Bay, greater boat traffic in combination with elevated water levels could increase the influence of these ship wake waves on beaches in the Bay (Leventhal and Baye, 2021).

ii. Tidal range and currents

Given comparable additional factors, macro-tidal shorelines have less beach-forming potential than micro-tidal conditions, since the period of wave influence on a specific elevation band is limited to a shorter time window. Tidal currents play a larger role in morphology than waves in these macro-tidal environments, where estuarine beaches are often wider and sandier. In micro-tidal conditions where waves are the dominant formation process and complex bar forms similar to ocean beaches are possible, beaches are typically narrower, with coarser sediment (Nordstrom, 1992).

San Francisco Bay exhibits a mixed, semi-diurnal tide, with two high tide and low tide peaks in a roughly 24-hr window. Tidal range can also vary significantly within a single estuary or basin, affecting the strength of tidal currents and the vertical distribution of wave energy (Nordstrom, 1992). The northern and southern ends of the Bay exhibit a higher tidal range than the Central Bay, a contributing factor for their relative lack of beaches.

Wind-driven storm surge can raise water levels within a basin well above the normal tidal range, and waves that would normally be dissipated by a low tide terrace have the capability of reaching the shore, resulting in episodic erosion events. Storm surge elevates the level of wave action to the normally dry beach berm or crest, so that post-storm, an estuarine beach form can be divided between a storm-sculpted upper foreshore and a daily-active lower foreshore (Jackson et al., 2002).

Longshore currents may be present on estuarine beaches at magnitudes even as great as ocean beaches, generated from sources including local wind waves, refracted swell, and tidal currents. These currents can be dominant agents of morphological change on low-energy beaches and may direct sediment transport on the low-tide terrace, such that different morphological agents exist on the upper foreshore and lower foreshore (Nordstrom, 1992). These currents are often strongest at headlands or channel constrictions (Nordstrom and Jackson, 2012).

Velocities and directions of currents in San Francisco Bay vary between sub-embayments, depending on river inflow, underlying bathymetry, and distance from the Golden Gate. In general, tidal currents are typically much stronger than freshwater flows in the Bay, and are responsible for significant bedform development, including west of the constricting Golden Gate, where decelerating currents cause sediment to deposit in an ebb-tidal delta that results in the San Francisco Bar, one of the largest sand wave fields in the world (Barnard et al., 2013). With higher freshwater inflow, northern sub-embayments can exhibit gravitational circulation, whereas the South Bay's limited freshwater input is insufficient to produce estuarine circulation cells (Conomos, 1979). Tidal currents are strongest within the Central Bay, which is also the deepest sub-embayment and contains the coarsest sediment (Barnard et al., 2013).

iii. Tidal flats

Another distinguishing feature of estuarine beaches is that they are often associated with a bayward mudflat, exhibiting a clear break in slope and sediment composition between the upper intertidal beach and lower intertidal mudflat (SFEI and Baye, 2020). Wave energy is dissipated in shallow waters over these tidal flats and waves often travel as spilling breakers towards the shoreline. In San Pablo Bay, wave heights can decrease by more than 50% across an extended mudflat (Lacy and MacVean, 2016). During lower and intermediate tides these tidal flats act as dampening agents to wave energy, so that only during water levels elevated by tide or storm surge does significant wave energy reach the active beachface. Thus, unlike ocean beaches where the sandy profile often extends to subtidal elevations, the window of

morphological change to an estuarine beach is limited by the tides. With increasing sea levels, waters will deepen over estuarine tidal flats, reducing their attenuation effect and increasing the window over a tidal range in which plunging breakers reach the beach shoreline.

The extent and elevation of mudflats vary throughout the Bay. They are less conspicuous in front of embayed, coarse-grained pocket beaches such as China Camp in Marin County, where plunging breakers can still occur at relatively lower tides (Nordstrom, 2022). Mudflats are more common in gently sloping, coastal plain basins such as the North and South Bay (SFEI and SPUR, 2019). Sediment composition within these tidal flats varies as well. At Greenwood Beach in Tiburon, the mudflat is a matrix of gravel, sand and fines, the result of stream deposition from a creek delta (Baye and Leventhal, 2020). Accretion of sediment to the beach from the low tide terrace is uncommon in BEBs due to the presence of water in tidal flats, which adds cohesion to the fine-grained sediment and makes sediment entrainment difficult. Short-period, proportionally steep, fetch-limited waves also have less ability to resuspend coarse sediment from tidal flats than swell waves (Goodfellow and Stephenson, 2005). However, whether some amount of the coarse fraction within these mudflats is released by wave action and transported to the beach is a subject of ongoing debate and research (Baye, personal communication, Nordstrom, 1992).

iv. Shoreline alignment

A governing characteristic shared with ocean beaches is shoreline alignment to dominant wave direction. Swash-aligned beaches are sites where the beach is oriented parallel to the dominant incident wave crest. This alignment encourages cross-shore transport as wave and swash processes move sediment landward or seaward along a beach's cross section. Alternatively, drift-aligned beaches are not parallel to the wave crest, so that waves approach the shoreline obliquely. This encourages longshore sediment transport as beach grains are forced down drift in the direction of the waves. While longshore transport rates are generally much lower on estuarine beaches than ocean beaches, the amount of sediment transported alongshore can comprise a higher proportion of the beach material present (Nordstrom and Jackson, 2012, Goodfellow and Stephenson, 2005, Jackson et al. 2002, SFEI and Baye, 2020).

The shoreline alignment along an estuarine beach can vary considerably across nearby sites and even within a single site. In addition to rocky headlands, urbanized / constructed features and stream mouths, substrate solidified by marsh vegetation can create outcrops where wave energy is not sufficient to cause erosion (Cooper et al., 2007). This is evident in historical imagery of Long Beach in San Leandro, where invasive cordgrass created micro-headlands and separated the beach into discrete sediment drift cells (SFEI and Baye, 2020). At Rat Cove Beach in Marin County, a 'hinge point' exists on the beach that is evidenced by the presence of bayfront vegetation on one half of the embayed shoreline, where an adjacent bluff presumably shields the area from higher wave action, as shown in Figure 4.

Figure 4. Rat Cove Beach (SFEI and Baye, 2020).

Wave refraction occurs less with short-period waves, and fetch-limited waves are often only weakly refracted by a shallow basin bottom before they are fully formed (Nordstrom and Jackson, 2012). Thus, the angle of wave approach to an estuarine beach is highly variable, both from the perspective of wave generation and shoreline orientation.

v. Sediment

The primary source supplying sediment to estuarine beaches can be a fluvial, such as a nearby stream or flood control channel, local, such as the erosion of a landward bluff, or offshore (sand through the Golden Gate or suspended sediment from the Bay in this regional context).

Sediment size and shape can offer clues towards a beach's incident wave conditions and geologic source. Coarse gravel beaches are typically found in shorter fetch conditions and contain substrate that is more challenging for vegetation establishment, whereas sandy, more

gently sloping beaches are often present in relatively higher energy contexts and can encourage vegetation establishment if wave energy is insufficient, as is shown in Fig. 4. More angular sediments are evidence of more recently eroded sources, whereas rounded grains signify longer, fluvial or glacial sources (Nordstrom, 1992, Pilkey, 2011). Beaches with these rounded sediments typically show higher longshore transport rates than angular sediment, although cross-shore sediment exchange for most estuarine beach sites is limited across sediment sizes (Nordstrom, 1992).

In addition to natural sources, anthropogenic sediment origins including dredge spoils or construction debris can serve as single- or multiple-event pulses that create or augment beach sediment supply. One example of this anthropogenic beach sediment source is Crown Beach in Alameda, the largest estuarine beach in San Francisco Bay. Although nourishment of the beach is infrequent, sediment distribution throughout the beach is an annual maintenance procedure; sand is dredged from either end of the drift cell and placed back near the center of the beach (EBRPD, 2013). The presence of concrete conglomerate or asphalt also highlights the erosion of a nearby levee or other manmade source in numerous S.F. Bay beaches.

Due to the widely varying geology, shoreline orientation and wave climate of S.F. Bay beaches, there is no typical grain size distribution among sites, and the median grain size, or D50, of a single site can even vary between ends of a single site. One example of this is seen at China Camp, where coarser, large gravel and boulder-sized sediment exists at the eastern end of the beach, with medium and fine sand present at the western end. This type of surface sediment

sorting can indicate a predominant direction of wave approach, with finer material being transported downdrift of coarser gravel and cobble.

Figure 5. China Camp Beach, 2021.

Right: western end, sand-dominated surface sediment. Left: eastern end, gravel and cobble-dominated sediment. (Left: sandy, gently sloping beachface with fine gravel toe, western edge.

Right: Concave, steeply sloping gravel beachface with storm berm, eastern edge.)

Shell is a lighter material that has more potential for migrating onshore from below mean sea level (MSL) (Nordstrom, 1992). Many beaches throughout the Bay contain shell fragments, and some are composed primarily of shell hash, such as the Bair Island Beach in Foster City.

Beaches are three-dimensional landforms, and the material of estuarine beaches frequently varies with depth. Coarser material often forms an immobile base layer under finer, sandier material, and may become exposed during beach erosion (Nordstrom, 1992), as finer material is more easily transported from the surface. In this manner upper foreshores of estuarine

beaches are often coarse, as relatively higher-energy events have the capacity to transport coarse material up the profile, and infrequent low-energy high tide events winnow away finer sediment. Coarse collections of sediment also form at swash excursions, sometimes shielded by wrack deposits, as well as at the beach toe, where finer sediment is winnowed away by swash drainage during low tide (Nordstrom, 1992). Outcroppings of clay or peat from buried marshes may also be present beneath the beach surface, creating pockets of impermeability which can increase sediment mobility through the lack of swash infiltration (Nordstrom, 1992, SFEI and Baye, 2020). Depending on the depth of the immobile base layer, which can vary in sediment composition from large cobbles to an impermeable clay matching the marsh material backshore, the active depth of the beach can be quite shallow, much shallower than the mixing depth typical of ocean beaches (Nordstrom, 1992).

vi. Biologic drivers of change

Biological activity can also play a role in altering beach composition. Vegetation can take hold along the shoreline where wave energy is not strong enough to erode the substrate, stabilizing sediment and acting as micro-headland features. Beach-stabilizing vegetation, whether in the cross-shore dimension at the crest of a beach, or in the longshore dimension of a beach, can act as retention structures during sediment transport events. Large woody debris is one example of both a naturally occurring feature and design intervention that helps retain sediment on estuarine beaches. Beach sediment can intergrade with backbarrier marsh substrate and bayward mudflat sediment, forming a continued beach system with distribution

of grain size and vegetation controlled by the presence of tidal range and wave energy. An abundance of driftwood, wrack vegetation and fine sediment in a beach system can also obscure the delineation between mudflat, beach, and salt marsh (SFEI and Baye, 2020).

Although marsh erosion is occurring in numerous locations throughout the Bay, this phenomenon has the potential to create beach features where interbedded marsh sediment is coarse enough to remain in place following removal by waves. In the Chesapeake Bay in Delaware, this process resulted in landward retreating marshes that form a bayward beach which transgresses at the pace of shoreline retreat (Maurmeyer, 1978). Unlike settings where high marsh habitat is eroded and transformed into low marsh habitat or mudflat, the presence of a beach can maintain a zone of high-tide refugia, where a specialized subset of plants and animals can thrive, including foraging habitat for shorebirds that don't have to expend as much energy leaving the shoreline when tides rise (Elsey-Quirk et al., 2019).

Another biologic factor that has the potential to influence estuarine shoreline morphology is invertebrate activity, through disruption of sediment structure on the beach or the intertidal mudflat. In San Francisco Bay, bat rays create small depressions in mudflats, and lugworms and ghost shrimp create small mounds of fine sediment through burrowing that can be mobilized more readily than an undisturbed tidal flat (DeWeerdt, 2022).

c. MORPHOLOGY

The morphology of estuarine beaches contains key differences from that of high-energy ocean beaches. California ocean beaches typically exhibit a seasonal profile cycle, wherein erosion occurs on the upper foreshore and deposition occurs on the lower foreshore during winter, high-energy conditions. During summer, accretion on the upper foreshore occurs as sediment migrates back up the beach profile in the form of a swash bar. In estuarine beaches, these cross-shore cycles of sediment transport are rare, especially with increasing tidal range. Morphological change is typically confined to the upper foreshore above the low tide terrace (Nordstrom, 1992). Permanent losses of sediment may occur offshore in estuarine beaches, particularly in fine sand beaches. The basic features of an estuarine beach section are shown in Figure 6.

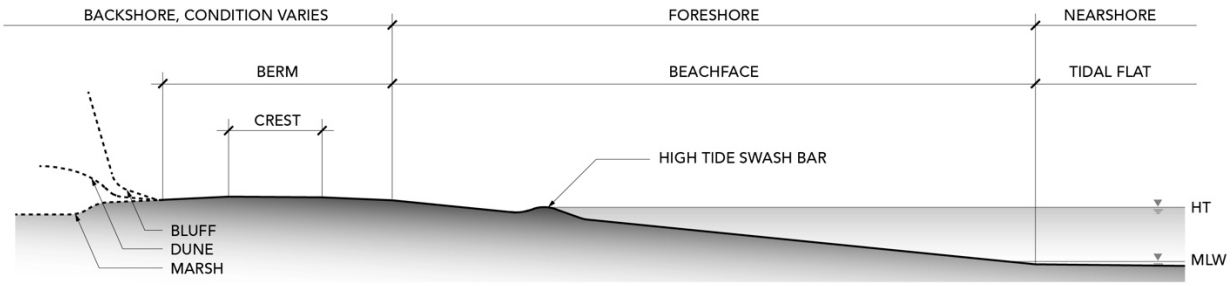

Figure 6. Typical estuarine beach section.

Instead of a seasonal cycle, meaningful morphological change at BEBs is typically limited to storm events, where wind and water level conditions combine to form waves with an energy great enough to transport sediment on the beach. These beaches often exhibit remnant

features, such as berms, scarps and washover deposits, from the previous storm event (or events). These features can persist for months, years or never fully 'recover' from erosion events due to lack of a replenishing sediment supply, human intervention, frequent storms, or low-frequency, 'beach-building' waves (SFEI and Baye, 2020, Gallop et al., 2020, Fellowes, T.E. et al., 2021). While estuarine beaches may experience accretion near stream mouths, inlets and other sources of sediment, they are typically eroding at rates faster than ocean beaches (Nordstrom, 1992).

Models for estuarine beach profile change in response to storm conditions are not as established as ocean beach models, profile response typologies have been offered by Nordstrom (1992) (Figure 7). One profile type, 'B1', is similar to the classic ocean erosion / deposition sequence, although with change confined to the upper foreshore above the low tide terrace. Where sites are exposed to longshore sources of sediment, this profile may be modified as a 'B2' type profile response, with a lower magnitude of profile change. A type 'C' profile response is identified by a parallel, more uniform slope retreat, which can signify the presence of longshore movement. These profile responses may occur in conjunction or at different times at the same site. In general, morphological change tends to be most pronounced at the boundaries of estuarine beach segments, whether this includes the end of the beach or a longshore barrier (Nordstrom, 1992).

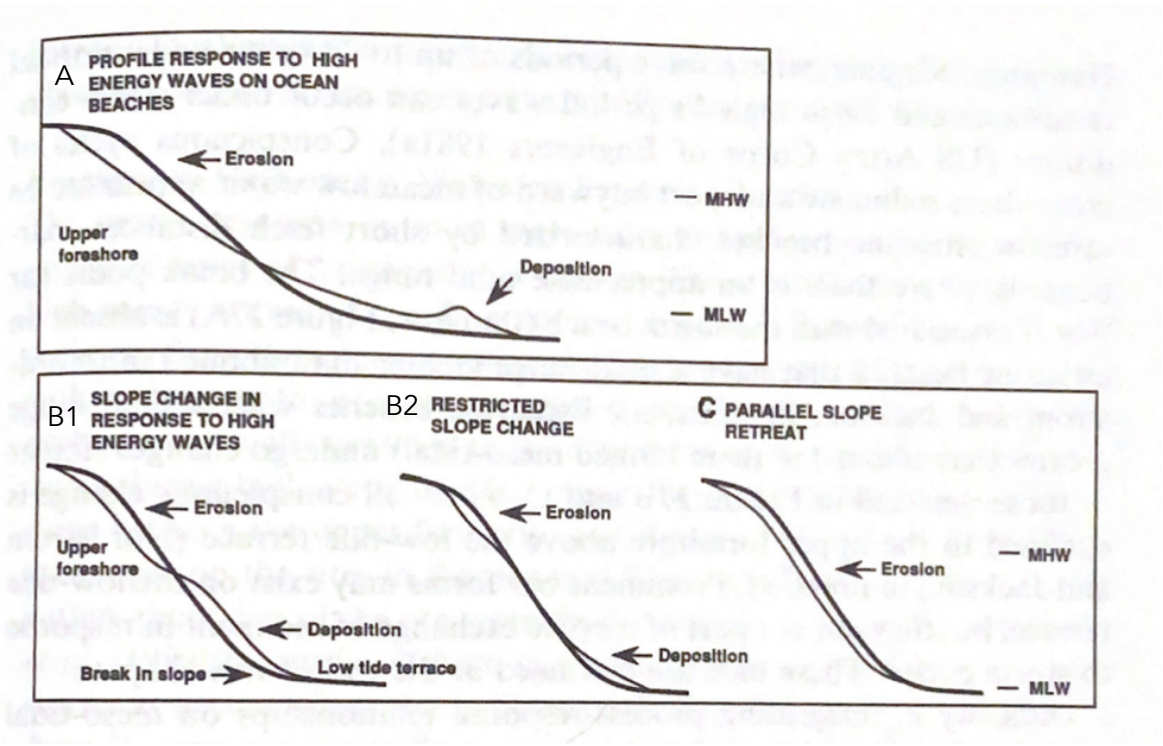

Figure 7. Profile response to erosional wave conditions on ocean and estuarine beaches. Modified from Nordstrom (1992).

Following sediment transport events, estuarine beaches can form a coarse-grained barrier that impounds smaller backbarrier drainage features similar to ocean beaches that close lagoon mouths in California during periods of low flow. In the Bay, this effect is seen most often at highly mobile shell beaches including Bair Island and Whittell Marsh. Closing off tidal channels in the absence of freshwater runoff can also result in the formation of salt pans behind the beach (SFEI and Baye, 2020).

Another morphological feature more commonly evident on ocean beaches but also present in estuarine beaches is washover deposits. In an ocean context, washover deposits are particularly

present along 'trailing-edge' coastlines such as the eastern United States and seen as a mechanism by which barrier island beaches migrate landward. As wave action pushes sediment over the beach crest, the sediment covers backbarrier marshes. As this process continues, the beach-sized sediment, more mobile, is continually pushed landward until it welds with the mainland, whereas the marsh sediment deposits often remain intact and eventually reveal themselves through the beachface (Pilkey, 2011). Washover deposits can consist of several different forms, including fans, terraces, or sheets, depending on the strength and alongshore distribution of wave energy, as well as the sediment composition of the beach (Morton and Sallenger Jr., 2003).

In an estuarine setting, washover is typically examined in the context of material deposited from an ocean beach behind its barrier, creating a lagoon-fronting shoreline of estuarine beach formed from washover deposits. However, sandy washover deposits have been shown to form high-tide islands, bars, or other refuge in tidally influenced environments (Cleary et al., 1979). Estuarine examples of washover deposits have been observed in Delaware Bay (Maurmeyer, 1978), lakes and reservoirs (Lorang and Stanford, 1993), and as thin layers deposited on backbarrier marshes at Long Beach and Point Pinole in San Francisco Bay (Baye, et al., 2020, SFEI and Baye, 2020). While referred to with varying terminology, this paper refers to the water overtopping a beach as "overwash" and the sediment deposited behind the crest of the beach as "washover."

III. STUDY SITE

Although numerous beaches were visited and considered for study, one site in particular was selected for study due to a combination of factors, including the presence of a backbarrier marsh and tidal flats, heterogeneous sediment composition, relatively long fetch and potential for strong wave events, unique formation process, adjacency to shoreline development, and general accessibility. In addition to making the site interesting to study in its own right, these characteristics make the chosen site a useful reference for other Bay beaches which may contain one or more of the listed elements.

Marina Bay Beach (also referred to as "the Beach") has no official name. It is a southwest facing beach located along the Richmond shoreline within the Central Bay of San Francisco (Figures 8a and 9). Its longest direct fetch is to the south, southwest towards the Bay Bridge and Treasure Island, reaching over 7 miles of fetch between 205 - 215° degrees (Figure 8b). It is bounded by a riprap embankment to the southeast and northwest, the latter serving as an edge to the San Francisco Bay Trail (Figures 9 and 10). The beach is approximately 300 feet in length, 90 feet in width and is the southern barrier of a small tidal marsh, which drains to the Bay via Meeker Slough. This tidal marsh, with a mouth approximately 1,000 feet northeast of the Beach, were part of a restoration effort in the 2000's to remediate industrial contamination present at the site (UCB, 2005). Presently, the marsh and Marina Bay Beach are publicly accessible and are frequented by pedestrians, dogs, and a variety of avian wildlife, including clapper rail and brown pelicans (NPS, 2010).

Figure 8a. Regional site setting, San Francisco Bay.

Box demarcates area shown in Fig. 8b

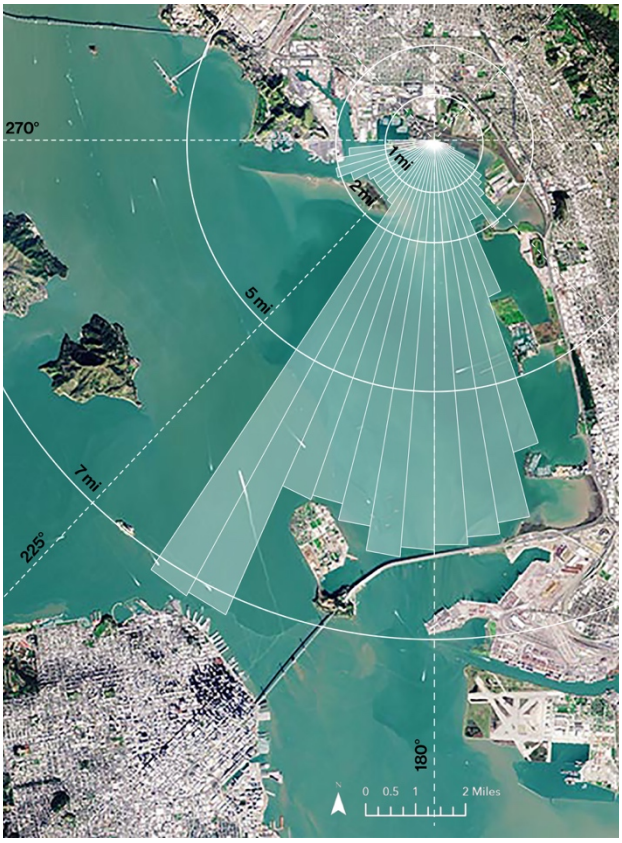

Figure 8b. Marina Bay fetch length, Central Bay.

(assuming no refraction)

Figure 9. Marina Bay site.

Figure 10. Marina Bay site (5 October 2021).

Looking from west end to riprap embankment at east end. Well defined beach berm with backbarrier marsh, cobble lag foreground.

A historic T-sheet from 1853 shows the protruding headland of with a sizable marsh behind it (Figure 11), and a linear edge of tidal marsh and grassland extending southeast (NOAA, 2016).

Figure 11. T-Sheet 399, 1853 overlaid on 2022 Richmond shoreline.

Marina Bay Beach site highlighted in yellow.

While this stretch of shoreline, a few hundred feet inland from the current footprint of Marina Bay Beach, could be a beach, it could also potentially represent a levee, protecting nearby plots of land indicated northward (Grossinger et al., 2005). A T-sheet from 1931 shows dramatic change (Figure 12); an industrialized waterfront filled into the Bay past the historic shoreline, with long breakwaters enclosing small marinas and bays.

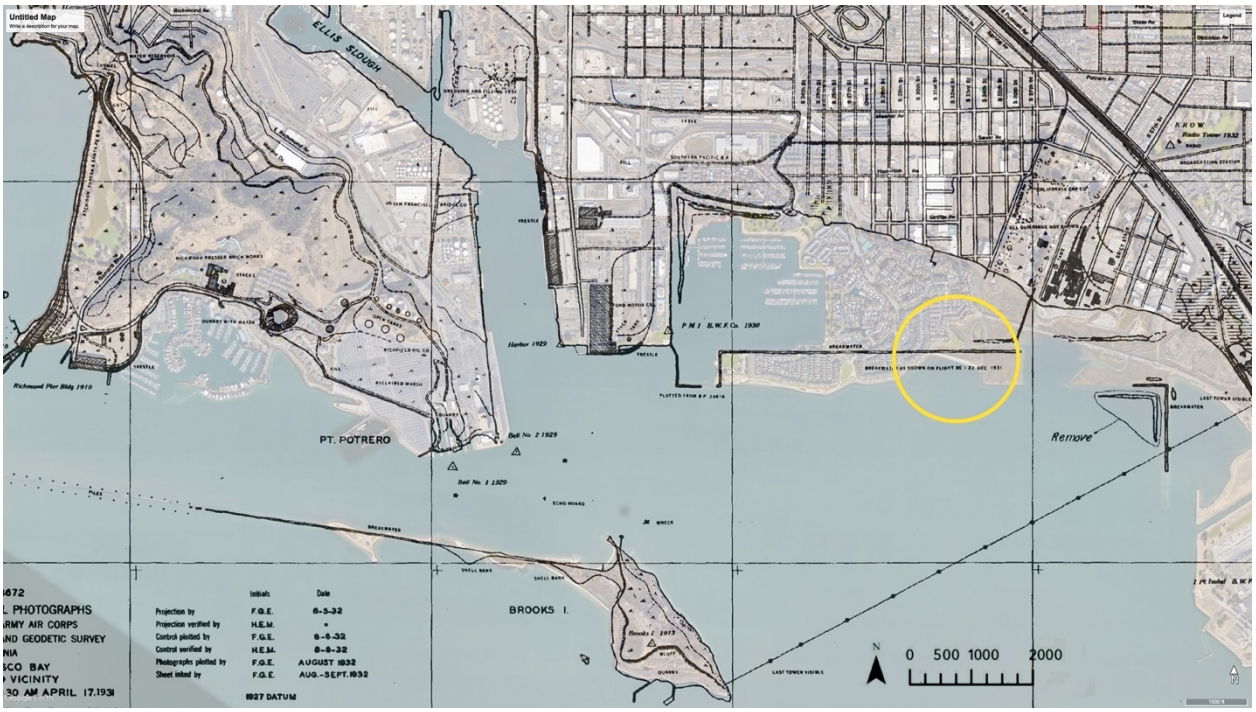

Figure 12. T-Sheet 4672, 1931 overlaid on 2022 Richmond shoreline.

Marina Bay Beach site highlighted in yellow.

The large tidal marsh behind Point Potrero has been channelized, and a quarry is established at another headland point, a precursor of the port that would occupy the former bluff's site. While crossed by a breakwater, the footprint of the present-day Marina Bay Beach is still located several hundred feet off the main shoreline in open water (NOAA, 2016).

The Kaiser Shipyards and other wartime production began dominating this stretch of Richmond shoreline in the late 1930s and 40s but following the declining use of the shipyards after WWII, a plan was made to redevelop this section of the Richmond waterfront as the Marina Bay neighborhood (NPS, 2020). In this planning process, a Special Area Plan (SAP) in 1987 shows

the conception of a beach along the entire southern shoreline of the residential Marina Bay development, where a riprap embankment to the Bay Trail now stands, as shown in Figure 13.

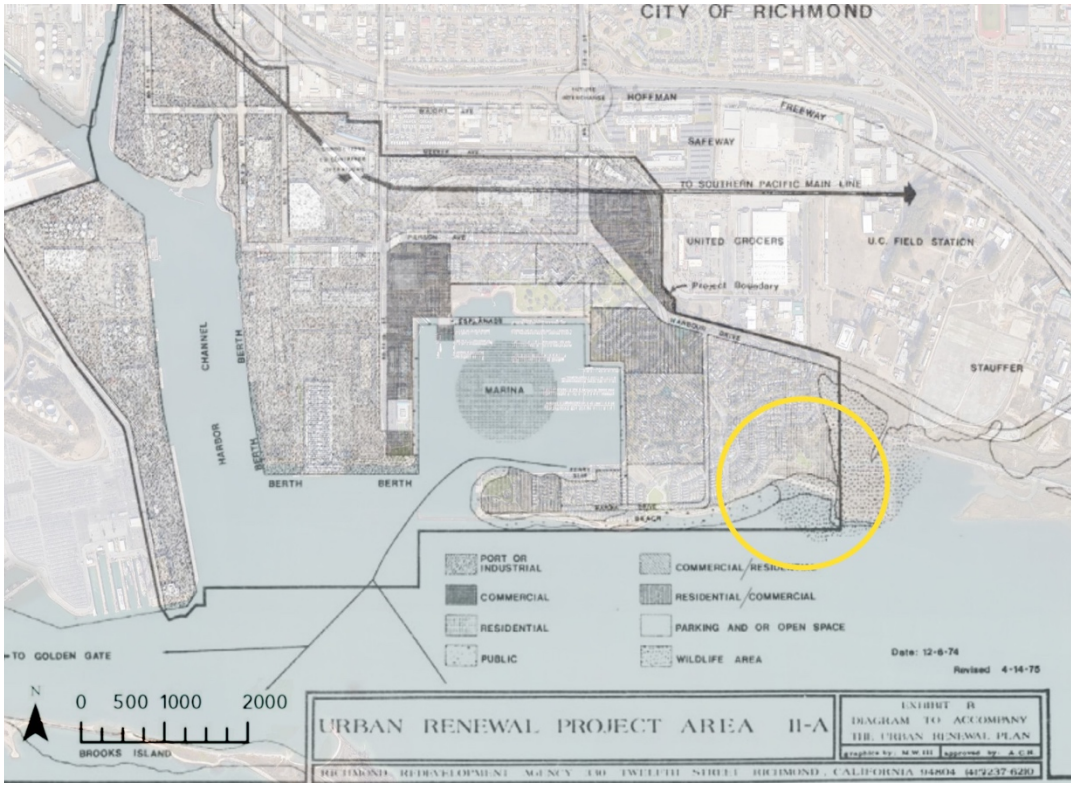

Figure 13. Richmond Inner Harbor Southern Shoreline Special Area Plan, 1987.

Marina Bay Beach site highlighted in yellow.

The material for this planned beach is conceivably sourced from local marine dredging and construction debris generated during the development. It is unknown why the plan for this more expansive beach was curtailed in favor of a riprap revetment against this southern edge of the Bay Trail, but concern for wave exposure and sediment transport was expressed in the 1987 SAP. In any case, a small stretch of beach was built close to what is shown in the "Wildlife Area" (Figure 13). It is unknown to what degree the beach was designed and engineered, but

personal communication (Baye, 2021) indicates that the area was largely a haphazard dump site of material that was later reworked by waves into a more stable beach form. As one example, a raised, conglomerate-based hillside on the eastern backshore of the current-day beach suggests a site of stockpiled excess material rather than an intentional landform.

IV. METHODOLOGY

Different methods were tested in order to evaluate various timescales of change. Annual or decadal beach morphology was evaluated using previously collected and published data, including wind and water levels and aerial imagery. Monthly or seasonal morphology was analyzed from data collected in the field, including topography and grain size analysis. Additionally, photographs, field notes and interviews of the site conducted every month during survey events helped reinforce and augment other data collection methods.

a. HISTORIC WIND AND WATER LEVELS

A National Oceanic and Atmospheric Administration (NOAA) monitoring station is located at Pt. Richmond on a pier that extends 500 ft into the Bay, approximately 3.6 miles northwest from Marina Bay Beach. Tidal datums for this site, which serve as approximations for the Beach, are shown in Table 1:

Table 1. Tidal Datum

Datum	Elevation (ft NAVD88)
Mean Higher High Water (MHHW)	6.06
Mean High Water (MHW)	5.45
Mean Tide Level (MTL)	3.30
Mean Low Water (MLW)	1.14
Mean Lower Low Water (MLLW)	0.02
Mean Range of Tide (MN)	4.33
Max Tide	8.65
Min Tide	-2.51

While it does not experience the same exposure and nearshore bathymetric conditions that the Beach does, this NOAA station is the closest source of historic wind and water level data for this site. Meteorological and water level records at this station exist as early as 2002 and starting in 2018 were collected as frequently as 6-minute intervals. For this study, wind speed and direction data were collected at 1-hr intervals for the entire available range, with the exception of years when meteorological data were not present (NOAA, 2022). A filter was created to identify potential wave conditions at Marina Beach, as outlined in Table 2:

Table 2. NOAA Station filter

Characteristic	Range
Wind Direction	90 – 270
Wind Speed	> 20 ft/s
Water Level	> 6 ft

These filter thresholds were developed as initial approximations for when significant waves could reach the Beach's shoreline. The 6 ft water level approximates the MHHW datum of 6.06' and the 90-270 degrees range represents a southern direction of long-fetch wind that could conceivably generate energetic waves at the Beach.

b. AERIAL IMAGERY

Remote sensing is useful in the analysis of beach and shoreline morphology. Numerous methods exist to identify shoreline location, beach slope, and other factors based on satellite

imagery datasets (Vos et al., 2019, Toure et al., 2019). These methods have been largely used on ocean beaches, which are typically much larger than estuarine beaches, although a couple studies have recently been conducted in San Francisco Bay, including that of SFEI and Baye (2022), and in Australia, from Fellowes et al. (2021). This study follows in those footsteps by using aerial imagery from Google Earth to track backshore changes in beach morphology throughout a twenty-year period.

Using Google Earth imagery as opposed to satellite imagery has several potential limitations and challenges. For one, imagery taken from Google is often mosaics of plane-based photography as opposed to satellite imagery and may contain horizontal distortions or inaccuracies. Additionally, Google Earth imagery is referenced only to a month and a year, as opposed to a specific day and time often found in satellite imagery sources. This makes it difficult to identify the tidal stage at which the image was taken.

Despite these limitations, Google Earth imagery was chosen as a method of aerial image analysis in this study for several reasons. Firstly, Sentinel satellite imagery was initially analyzed through the satellite subscription service Planet. However, the finest resolution available is 9.84 ft (3 m) pixel size, and even with sub-pixel analysis, the resolution is too coarse to capture the small scale of Marina Bay Beach, 900 feet in the longest direction. Secondly, although a specific datetime stamp would be crucial for evaluating shoreline evolution, backbarrier subaerial features at the study site are almost always completely exposed at most tidal stages and are thus not as sensitive to this limitation. Finally, although imagery from only a few

months of select years exists on Google Earth, it contains a longer, consistent historical record than publicly available, 3.28 ft (1pm) pixel-sized satellite imagery, and can provide a monthly-, seasonal-, or annual-scale perspective of morphological beach change.

Following a procedure outlined in Shifting Shorelines (SFEI and Baye, 2022), aerial images were extracted from Google Earth and georeferenced into ArcGIS. At least one image was extracted for every year of available data from 2004 to 2022 with the exception of 2006, where only one available image was obscured by cloud cover. An unsupervised image classification procedure was utilized to identify pixels of similar color, aiming to highlight beach-colored pixels. These pixels were cropped to a standard boundary that excluded deviations in tidal stage, and adjacent areas with similar pixel colors, including the Bay Trail path and neighboring marsh. The area of these pixels was then calculated and compared with other years. During years following expected events with washover deposits, more beach-colored pixels were exposed, owing to recent deposition behind the beach crest. Over the following months and years, this washover sediment is recolonized by beach and marsh vegetation, shielding them from aerial imagery, so that in years with no washover deposits, subaerial beach area is smaller. Through this procedure, the beach area is expected to correspond positively with storm conditions (high winds in the direction aligned with high water levels), given a lag due to time in collection and posting of Google Earth aerial imagery.

c. WAVE DATA

A pressure transducer was installed on the tidal flat fronting Marina Bay Beach, 200 ft from the toe of the Beach and aligned approximately with the center of the Beach. It was deployed from 22 April until 22 June 2022, with the device set at a measuring frequency of 2 Hz. Upon data recovery, it was discovered that data from 17 May to 4 June 2022 was not recorded (see Fig. 24 in Results). Pressure values were converted to water depth via Equation 1:

$$h(t) = \frac{p_r(t) - p_b(t)}{\rho(t)g} + z_I \qquad 1$$

where g represents gravity, ρ represents the density of seawater, assumed at 64 lb./ft^3, p_r represents the pressure logged by the transducer, p_b represents the atmospheric pressure, z_I represents the height of the transducer above the surrounding mudflat grade, and $h(t)$ represents water level as height above mudflat h at a given time t. The tidally varying water depths were compared to verified water levels from the NOAA Pt Richmond Station at 6-minute intervals, converted from a MLLW datum to a NAVD88 datum. Running average and standard deviations statistics of both the measured and NOAA-sourced water level data were taken using one hour time segments (10 data points for the NOAA data, 7200 data points for the measured data) to produce a water level record, represented by an hourly average, and a wave record, represented by an hourly standard deviation. To compare wave results against meteorological forcing, wind speed and direction data were also gathered from the NOAA Pt.

Richmond Station at 6-minute intervals, averaged with a moving mean sampling 10 data points to produce an hourly average.

To estimate the significant wave height *Hs* of the data collected from the pressure transducer, a frequency analysis approach following WinklerPrins et al. (2021) was used. First, the data were divided into 6-minute subsets for a total of 719 measurements in one subset, in order to align with the frequency of the NOAA station measurements. A frequency cutoff was imposed in order to eliminate noise from the wave record using Equation 2, where given frequencies *f* exceeded the cutoff frequency f_c:

$$f_c = \sqrt{\frac{g}{4\pi(h - z_I)}} \qquad 2$$

where h-z_I represent depth of sensor below the water surface. A translation between surface and depth spectra (Equation 3) was included to account for a weakening pressure signal with depth:

$$S_\eta(f) = \left[\frac{N(f)}{K_P(f)}\right]^2 S_d(f) \qquad 3$$

Where $S_d(f)$ and $S_n(f)$ represent the depth and surface-height spectra, N is an empirical correction factor set to 1 per Bishop and Donelan (1987) and WinklerPrins et al. (2021), and $K_p(f)$ is the pressure response factor, calculated as:

$$K_p = \frac{\cosh k(h - z_I)}{\cosh kd} \quad (4)$$

where k represents the wavenumber. With the surface height spectrum known, the significant wave height Hs for each 6-minute segment is found with Equation 5:

$$Hs = 4\sqrt{m_0} \quad (5)$$

where m_0 is the 0th spectral moment. The significant wave period T for each spectrum was then calculated as:

$$T = \sqrt{\frac{m_0}{m_2}} \quad (6)$$

where m_2 is the 2nd spectral moment. These Hs and T values were compared to formula from the US Army Corps of Engineer's Shore Protection Manual (USACE, 1984) relating to fetch-limited waves, where Hs_{theory} is estimated as:

$$\frac{gHs_{theory}}{U^2} = 0.283 \tanh\left[0.530 * \left(\frac{gd}{U^2}\right)^{\frac{3}{4}}\right] \tanh\left\{\frac{0.00565\left(\frac{gF}{U^2}\right)^{\frac{1}{2}}}{tanh\left[0.530\left(\frac{gd}{U^2}\right)^{\frac{3}{4}}\right]}\right\} \quad 7$$

and T_{theory} is estimated as:

$$\frac{gT_{theory}}{U} = 7.54 \tanh\left[0.833 * \left(\frac{gd}{U^2}\right)^{\frac{3}{8}}\right] \tanh\left\{\frac{0.0379\left(\frac{gF}{U^2}\right)^{\frac{1}{3}}}{tanh\left[0.833\left(\frac{gd}{U^2}\right)^{\frac{3}{8}}\right]}\right\} \quad 8$$

Differences between measured and theoretical results were analyzed, as well as the correlation between water level and wind forcing.

d. TOPOGRAPHIC TRANSECTS

Over the course of eight months, four transects were surveyed along the beach a total of eight times each. These transects were not evenly spaced along the beach but were positioned to take advantage of specific site features, as shown in Figure 14.

Figure 14. Site map of transect locations.

Transect 1 ("T-1") is located at the eastern end of the Beach, at a low bluff that exhibits a conglomerate of erosion-resistant material, likely a concentration of dumped debris. Transect 2 ("T-2") is close to the center of the beach, selected as a representative, normative condition that is displayed along much of the beach of a sandy, vegetated crest and a sloping sandy backshore that intergrades with the backbarrier marsh. Transect 3 ("T-3") is aligned with a tidal pond feature in the backbarrier marsh, the terminus of a tidal channel. Transect 4 ("T-4") is the western-most transect, originally positioned at a low point in the beach crest, where much coarser material was present.

These transects were surveyed with an Emlid Reachview 3 Real Time Kinematic ("RTK") system following a general procedure for topographic surveys stated in Bracewell (2017). The first four surveys, from 19 October 2021 to 20 January 2022, were surveyed using the RTK's base station

method, and the remaining four surveys, from 26 March 2022 to 26 June 2022, were collected using a NTRIP system from the CRTN network. At least eight reference points were logged during each survey event, as well as occasional surveys of a nearby NGS benchmark DE8481, in order to correct minor anomalies in survey data between events.

e. TRACER STUDY

To carry out a tracer study of beach sediment transport, a range of sediment sizes was first collected from the Beach, ranging from fine sand and silt to large gravel and shell and weighing approximately 25 lb. This sediment was prepared as a tracer by dying using an "Invisible Blue" fluorescent pigment, which was rinsed and dried, following the procedure outlined in Kinsman and Xu (2012). The sediment was then distributed in a 2' x 5' area on the Beach on 26 May 2022, aligned with T-3 at the mid beachface. This location was selected since there was evidence of washover deposits in the backshore condition (see Topographic Transects in 'Results'), implying the potential for cross shore transport, and from grain size analysis, qualitative observations of litter patterns and discussions with local residents, there was an initial expectation that longshore transport was directed from west to east. Placement of the tracer along the T-4 transect, although containing the characteristics noted above, was not preferred due to the non-representative grain size and slope that this transect represented. Additionally, T-4 is closest to the Bay Trail and contained more potential for disturbance from pedestrians. Thus, placement of the tracer at T-3 was intended to allow the potential capture of both cross-shore and longshore transport.

Following placement, the tracer was covered with a 0.5" layer of surrounding, undyed sediment to minimize movement due to surface effects such as wind and pedestrian movement. The tracer movement was measured for four tidal cycles following deployment during low tide, at approximately 24-hour intervals, and once more at the end of the study period three weeks later on 12 June 2022. During survey events, the Beach was swept in cross sections spaced at approximately 2', with a UV flashlight used to illuminate the beach surface. The presence of visible dyed grains was logged using the RTK survey equipment. These points were then imported into ArcGIS to calculate the center of mass for each survey date. Additionally, the T-3 transect was surveyed during each visit in order to aid in correlating the interpretation of cross-shore changes gathered by the transect surveys to the longshore changes expected to be gathered by the tracer study.

Figure 15. Tracer study methodology images.

(Left: tracer preparation. Center: tracer deployment. Right: tracer survey, 24 May 2022)

f. GRAIN SIZE ANLAYSIS

During three separate survey events (16 October 2021, 26 March 2022, and 26 June 2022), grain samples were collected from the Beach. This process, following a procedure outlined in Bunte and Abt (2001), was intended to characterize the sediment composition along each surveyed transect. For each transect, three or four representative locations were selected of relatively homogenous sediment composition. One sampling location was typically positioned on the beach berm, one on the beachface, and one at the beach toe, which were often representative locations of different zones of sediment composition. These designated sampling locations were logged by the RTK survey equipment. Enough sediment was collected from the top 2" of the beach surface to fill a 6" x 6" Ziploc bag, approximately 1 lb. of material (Figure 16).

Figure 16. Site sediment observations.

Left: old Bay mud outcrop on western lower beachface. Center: sediment collection bags. Right: Well-sorted shell scarp on western upper beachface, 19 October 2021.

These samples were then dried in an oven to remove water content and sieved. The samples were separated into ten different classes corresponding to the Wentworth scale as shown in Table 3, with quantities calculated including D50 (Wentworth, 1922).

Table 3. Grain Size Analysis Classification

Phi (Φ)	Sieve Size (mm)	Sediment Class
-4.5	22	Coarse gravel
-4	16	Coarse gravel
-3	8	Medium gravel
-2	4	Fine gravel
-1	2	Very fine gravel
0	1	Very coarse sand
1	0.5	Coarse sand
2	0.25	Medium sand
3	0.125	Fine sand
4	0.063	Very fine sand
	< 0.063	Fines

V. RESULTS

The following sub-sections cover the data gathered from the different methods. As they represented the majority of morphological change observable on site, washover deposits formed during the field surveying period and periodically throughout previous decades were central features of analysis. As is shown, these washover fans are most often present landward of the beach berm, depositing into the backbarrier marsh. Data collected during periods in which washover fans were not detected, including the wave data, tracer study and numerous transects, are also included as a contrast to the conditions capable of producing these morphological features.

Results from field survey methods were highlighted by a significant storm event on 24 October 2021. At NOAA Pt. Richmond station, water levels exceeded 7 ft, associated with winds exceeding 40 ft/s and persisting between 140-160 degrees, representing a storm surge of 1.7 ft (Figure 17).

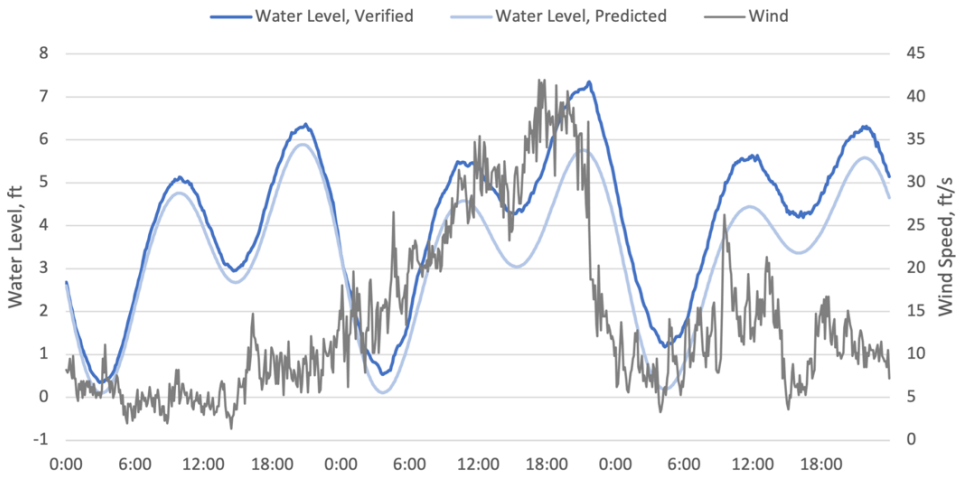

Figure 17a. 24 October 2021 storm event wind speed and water levels.

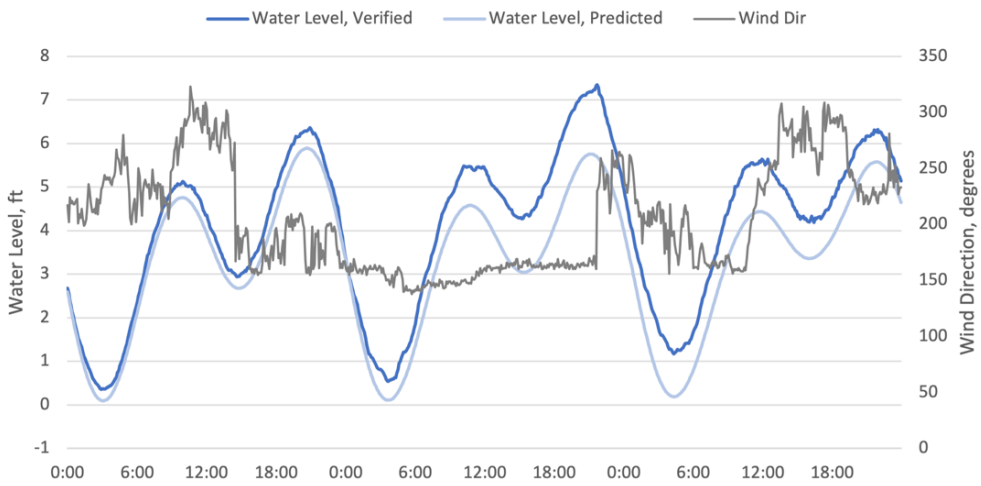

Figure 17b. 24 October 2021 storm event wind direction and water levels.

The combination of these sustained winds, increasing in speed along with rising water levels, created waves at Marina Bay Beach strong enough to alter beach morphology. Photos of the breach during this storm were captured by resident Karen Barad (Figures 18a-b).

Figure 18a. 24 October 2021 Storm event, looking south towards San Francisco Bay.

Waves overwashing beach on western end of Marina Bay Beach. Largest overtopping at far left observed at location of subsequent washover fan.

Figure 18b. 24 October 2021 Storm event, looking south towards San Francisco Bay.

Water levels elevated in marsh, beach crest exposed. Beach sheltering wave energy from S.F. Bay.

One survey event was conducted five days prior to the storm on 19 October 2021, and the next survey was on 30 October 2021, six days after the storm. These two dates typically display the most change across each survey methodology chosen. However, subsequent monitoring in following months represent notable instances of stability or gradual adjustment on the Beach.

a. HISTORIC WIND AND WATER LEVELS

Average monthly wind speeds, collected from 1997-2022 from the NOAA station in Pt. Richmond, are shown in Table 4.

Table 4. Average Monthly Wind Speeds, NOAA Pt. Richmond Station

Month	Jan	Feb	Mar	Apr	May	Jun	Jul	Aug	Sep	Oct	Nov	Dec
Avg. Wind Speed (ft/s)	16.75	17.00	16.32	18.02	17.10	17.27	16.79	15.52	13.36	13.59	15.36	16.94

Contrary to expectation, higher average monthly wind speeds occur in spring months (April, May, and June), with lower average winds occurring in autumn (September, October, and November). Typical 'storm months' of December, January, and February exhibit winds close to average for the site of 16.17 ft/s. A wind rose for the Pt. Richmond station, exhibiting data from the 1997-2022 collection window, is shown in Figure 19 below.

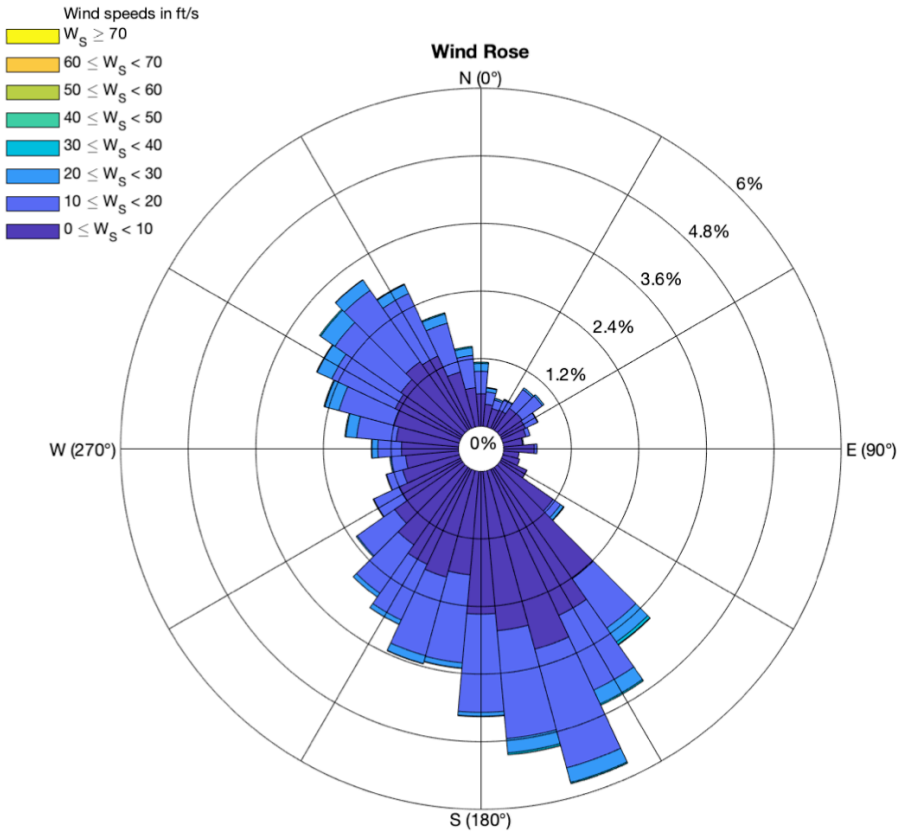

Figure 19. Wind Rose, NOAA Pt. Richmond Station

The wind rose shows that most wind travels from the south-southeast, approximately 170 degrees. Additionally, wind directions associated with water level tidal residuals of 0.5 ft or greater were binned and sorted over the period of data collection (Figure 20).

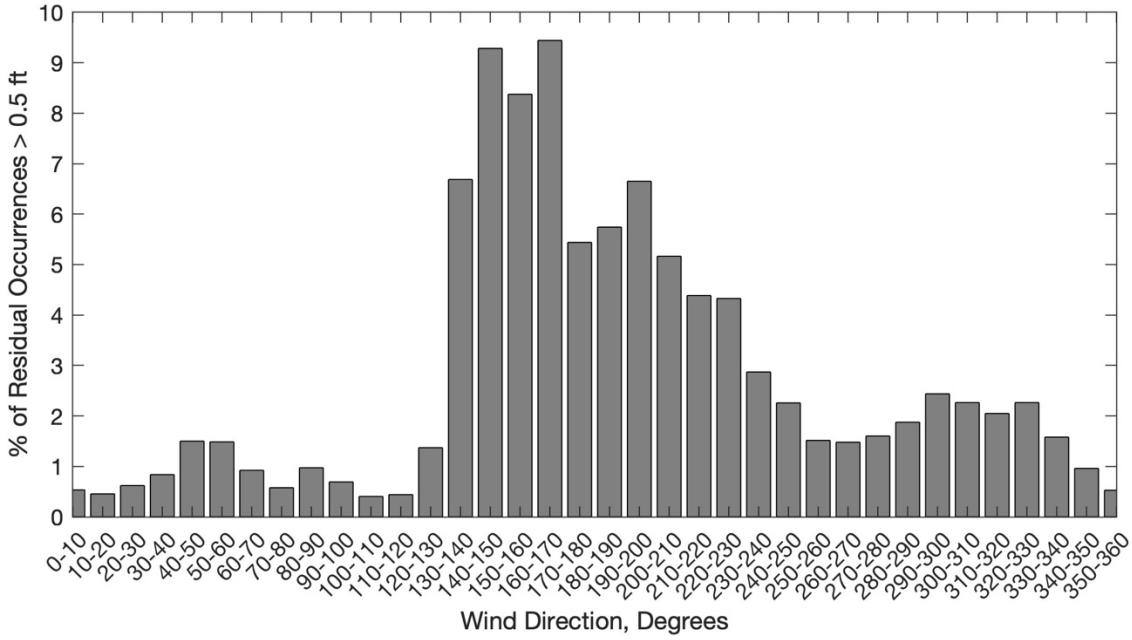

Figure 20. Historical wind direction and residual correlation, NOAA Pt. Richmond station. Percentage of all >0.5' residual events that fall within a 10-degree band of wind direction.

Positive water level residuals typically occur from winds that approach the site from 140 – 170 degrees, with still significant percentage of residual occurrences seen up to 230 degrees and as low as 130 degrees.

b. AERIAL IMAGERY

Results from historic aerial imagery subaerial beach area analysis are shown in Table 5 and Figures 21 and 23, as well as Figures A1a-y in Appendix A. A composite of all years is shown in Figure 22.

Table 5. Subaerial Beach Area

Date	1993.07	2002.10	2003.07	2003.12	2004.09	2005.04	2005.09	2006.--	2007.05
Beach Area (sf)	79,181	79,990	81,585	80,885	79,548	83,071	80,008	---------	81,820
Date	2007.06	2008.04	2009.10	2010.07	2011.10	2012.08	2013.04	2014.03	2015.04
Beach Area (sf)	85,541	84,572	77,874	78,688	78,349	76,150	78,251	75,998	79,048
Date	2016.03	2016.11	2017.03	2018.03	2019.06	2020.08	2021.02	2022.02	
Beach Area (sf)	78,550	82,063	79,596	81,254	82,256	76,855	78,348	76,474	

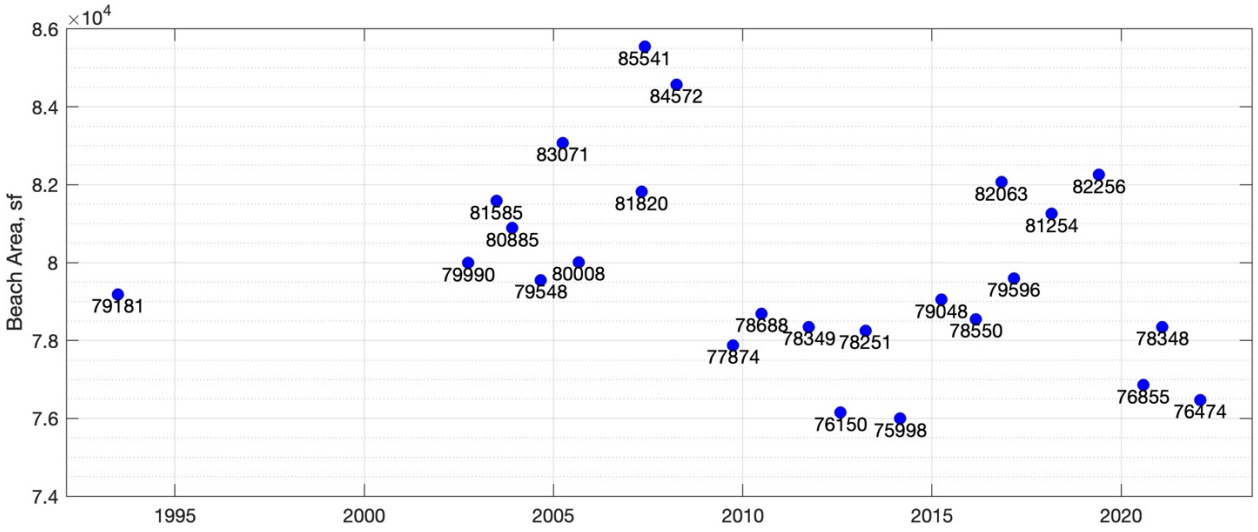

Figure 21. Subaerial Beach Area, 1993-2022.

Figure 22. Composite subaerial beach area.

Yellow shading represents subaerial beach area, overlaid from all years of analyzed data. Solid color represents overlapped area between imagery.

The imagery analyzed yields quantifiable change in subaerially-exposed beach area throughout the roughly twenty-year study period. Conspicuous increases in beach area occur between 2002 and 2003, 2005 and 2006, 2008 and 2009, and 2018 and 2019. While substantial ranges of missing data from the Pt. Richmond NOAA station preclude comparison between historic wind conditions and subaerial beach area, comparison with water level data is possible, as those records are more consistent at the Pt. Richmond station (Figure 23).

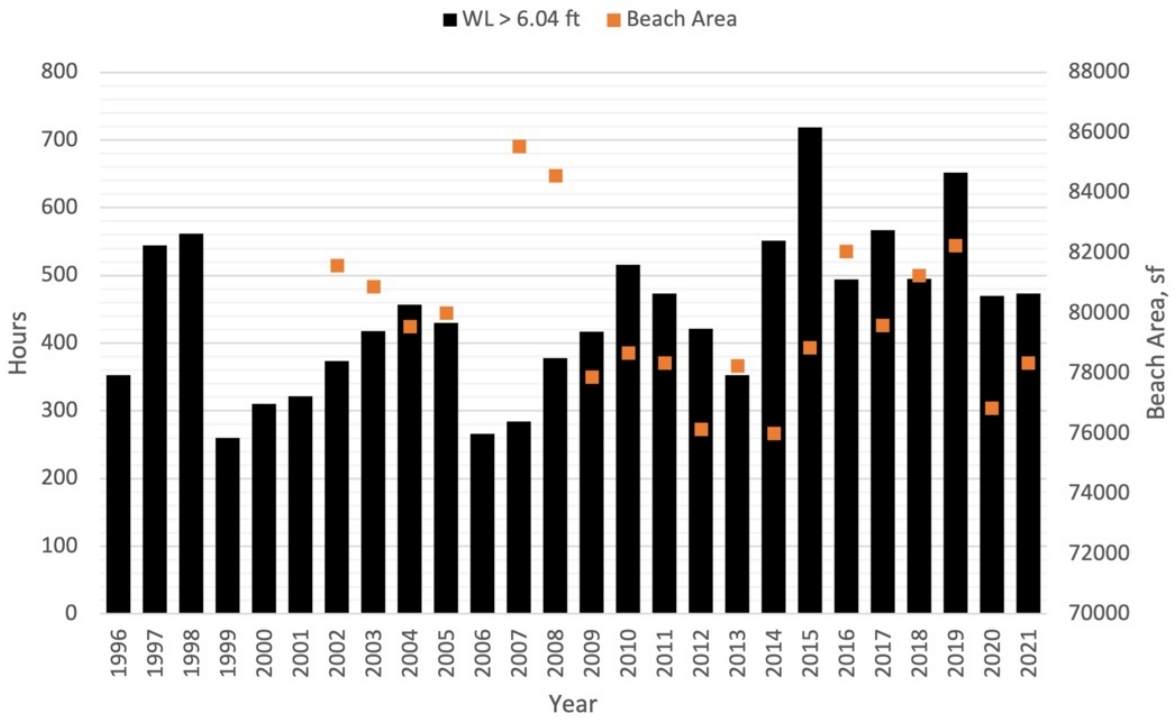

Figure 23. Subaerial beach area.

Number of hours in year in which water level exceeds MHHW represented in black bars. Subaerial beach area represented in orange squares.

Fig. 23 uses MHHW at the Beach as a minimum threshold filter for conditions when significant waves could occur. Conceptually, more elevated water levels should signify more opportunities for significant storm events to occur and a greater chance of washover deposits, and thus a larger beach area in the following year. This is evident in some years in Fig. 23, such as 2004-2005, 2014-2015, and 2017-2018, when a corresponding relationship between high water level occurrences and beach area is present. However, the trend largely doesn't hold for most years throughout the period of data analysis.

c. WAVE DATA

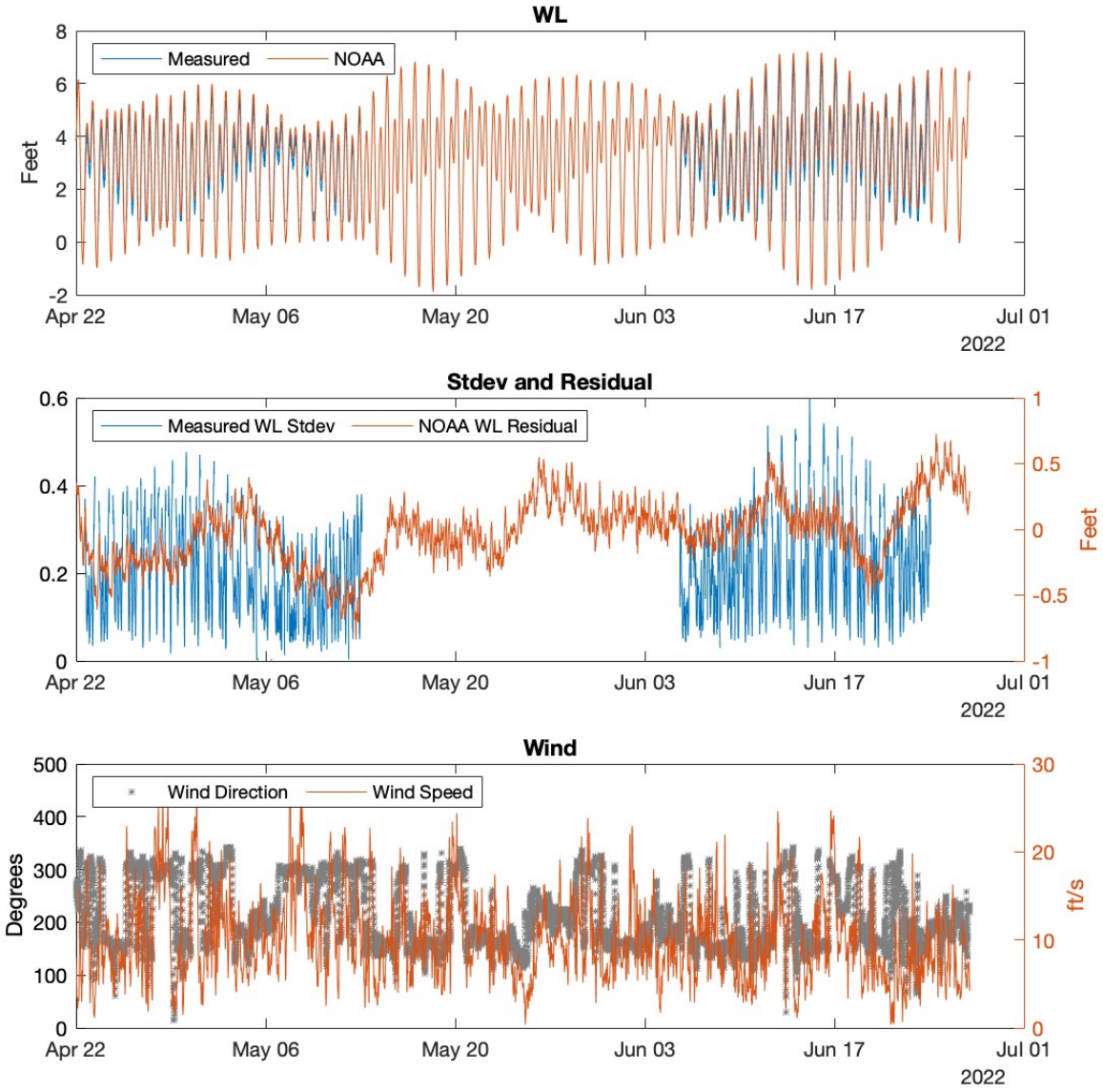

Figure 24. Water Level and Wind Data during Wave Gauge Deployment

In top panel, orange lines represent verified water levels from the NOAA Pt. Richmond station, and blue lines represent water levels measured from the pressure transducer. In center panel, the orange line represents the difference between predicted and verified water levels from the NOAA Pt. Richmond station, and the blue line represents standard deviation of water levels measured from pressure transducer. In bottom panel, the orange line represents wind speed and gray dots represent wind direction, both measured from the NOAA Pt. Richmond Station.

Several comparison plots were conducted using NOAA Pt. Richmond data and measured wave data in order to establish general trends and variable correlations. Figure 24 displays all data collected during the study period. In the "WL" subplot, measured water level values have been converted from pressure readings and are compared to NOAA water level readings from the Pt. Richmond station, with the gap of measured water levels seen between 17 May 2022 and 4 June 2022.

As described in Methodology, measured *Hs* values were calculated via a frequency analysis for 6-minute ranges. These values were classified into three different height classes proportional for the waves observed – relatively high waves (> 0.66 ft), medium waves (0.33 – 0.66 ft), and low waves (<0.33 ft). All spectra for these segments were plotted, along with class averages, in Figures 25a-c.

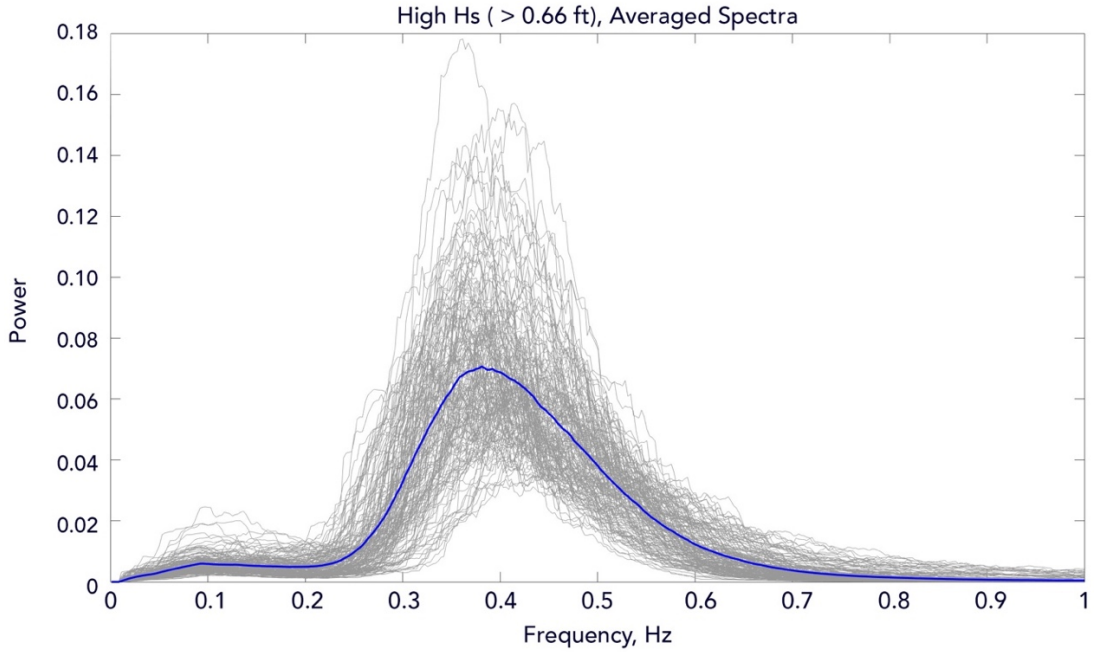

Figure 25a. High Hs averaged spectral curve. Gray lines represent a single spectral curve, blue line represents average of all high Hs spectra.

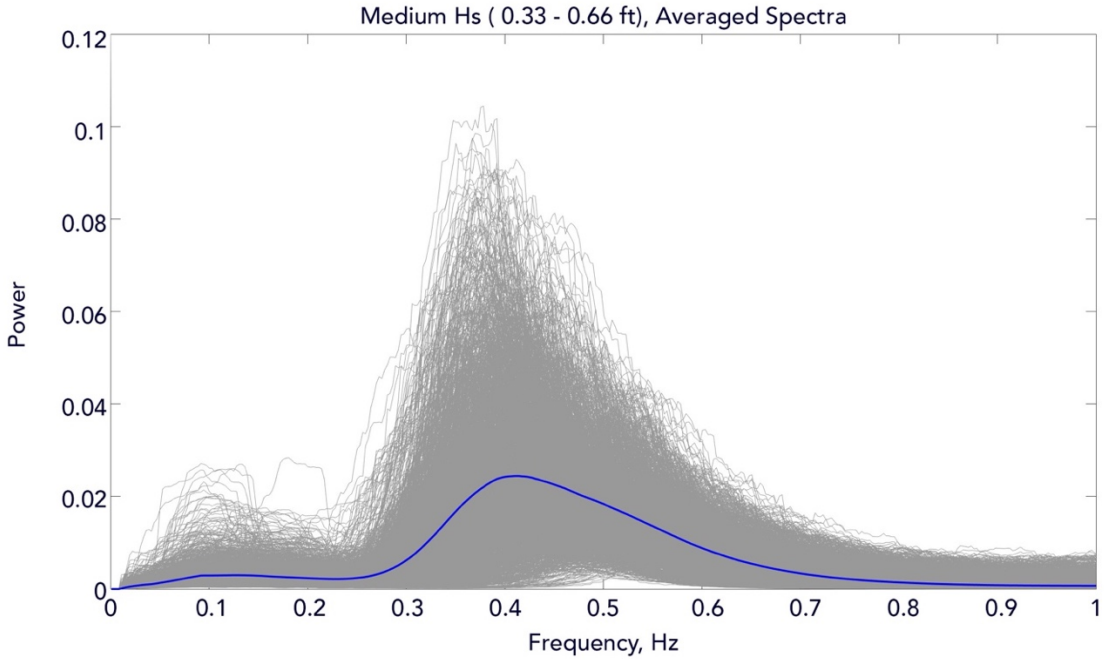

Figure 25b. Medium Hs averaged spectral curve. Gray lines represent a single spectral curve, blue line represents average of all medium Hs spectra.

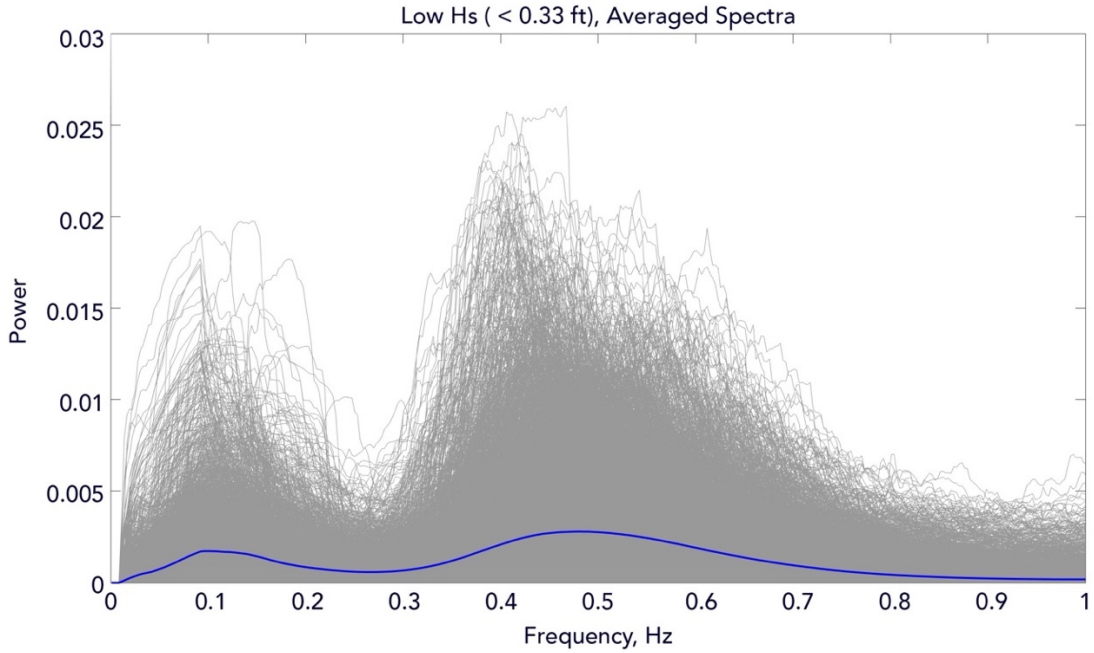

Figure 25c. Low Hs averaged spectral curve. Gray lines represent a single spectral curve, blue line represents average of all low Hs spectra.

All three wave height classes display average frequency peaks between 0.35 and 0.50 Hz, increasing slightly as the wave height decreases. This frequency peak range represent periods of 2.86 and 2 seconds respectively and is consistent with the wind-wave spectrum observed in Tomales Bay by WinklerPrins et al. (2021) and in Botany Bay by Rahbani et al. (2022). High, medium, and low *Hs* waves exhibit average power peaks of approximately 0.07, 0.025, and 0.003, respectively. Also, the relative contribution of low frequency energy, seen by a local peak at approximately 0.1 Hz, increases as wave height decreases. Although some estuarine beaches exist in San Francisco Bay that are likely to have swell influence, for this study Marina Bay Beach was analyzed assuming that all waves were locally generated, with swell having

been dissipated primarily through the Golden Gate, and across the narrow bathymetry and other headland obstructions leading towards the Beach.

A time series comparison between measured *Hs* values and *Hs* values calculated from the USACE Shore Protection Manual, separated into the two ranges of viable wave gage data, are shown in Figure 26.

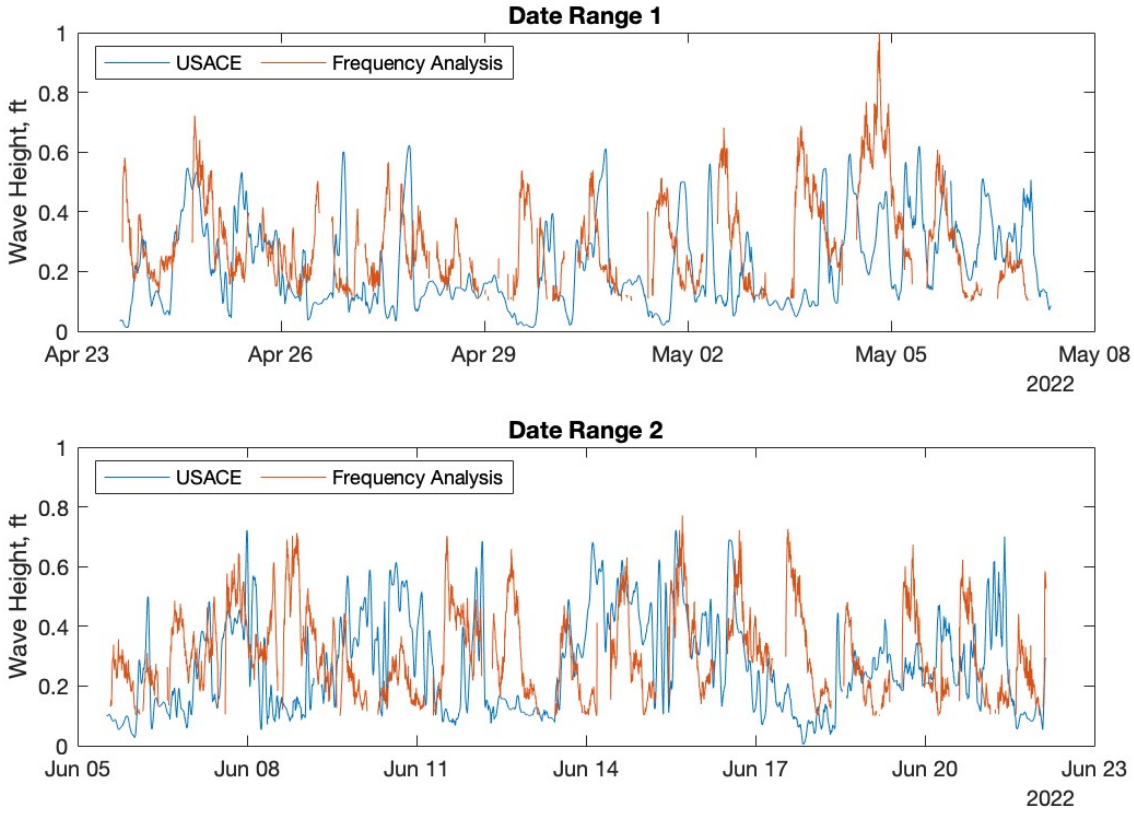

Figure 26. Comparison between measured and theoretical Hs values.

Date ranges separated by periods of viable wave gage data.

As these comparison plots show, both measured and theoretical significant wave heights have similar orders of magnitude, ranging from 0.1 ft to a maximum of 1.0 ft, but seldom exceeding

0.7 ft in height. This is consistent with wave heights seen in low-energy beaches during calm conditions as defined by Jackson et al. (2002). However, the methodologies display a poor agreement, with non-coinciding spikes of higher wave heights. To investigate this discrepancy further, scatter plots in Figures 27a-c display the comparisons between each Hs method and the wind direction, wind speed, and water level.

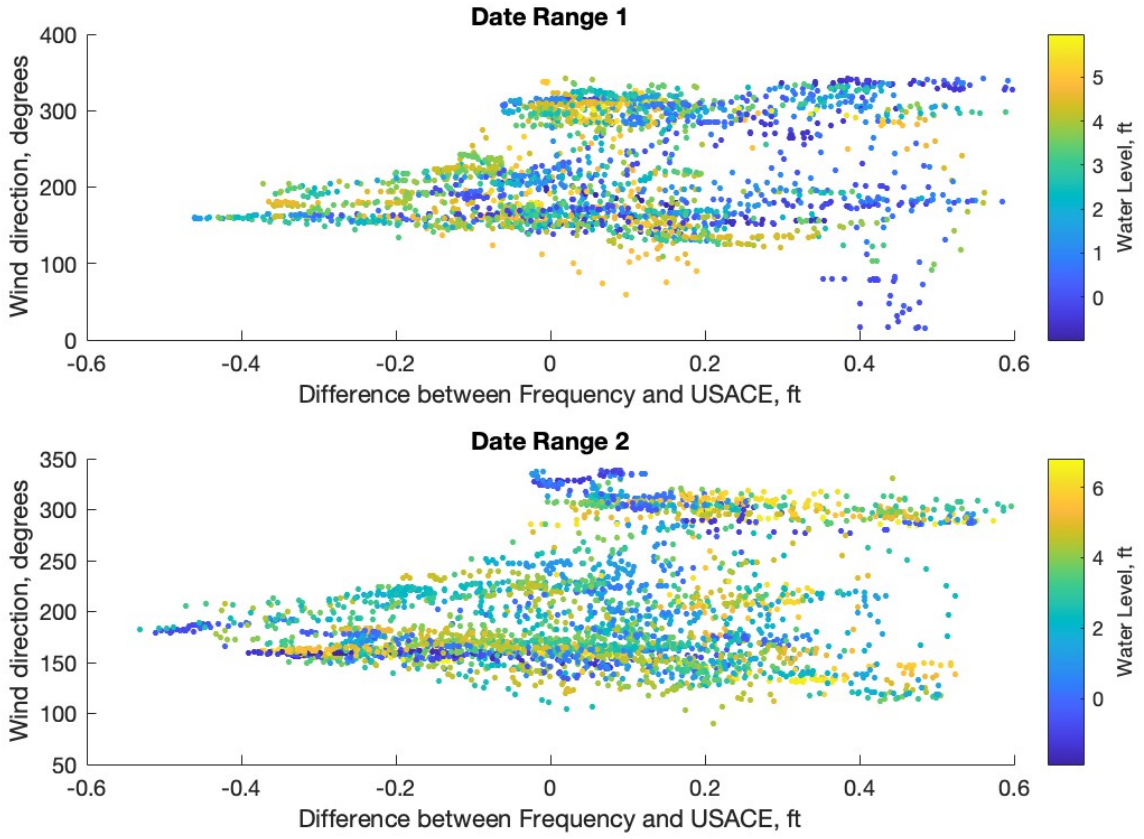

Figure 27a. Correlation between differences of Hs measurements and wind direction, water level. Color gradient represents water level. Date ranges separated by periods of viable wave gage data.

In Date Range 1 of Fig. 27a, it appears that generally lower water levels during both southerly (~170 degree) winds and northerly (~310 degree) winds result in a higher measured Hs than

the theoretical USACE equations account for. Conversely, medium- and high-water levels in the shore-incident 150-200 degree range are largely underpredicted by the USACE equations in this date range. However, this trend doesn't hold for Date Range 2, with higher measured water levels and significant wave heights underpredicted in the theoretical USACE equations.

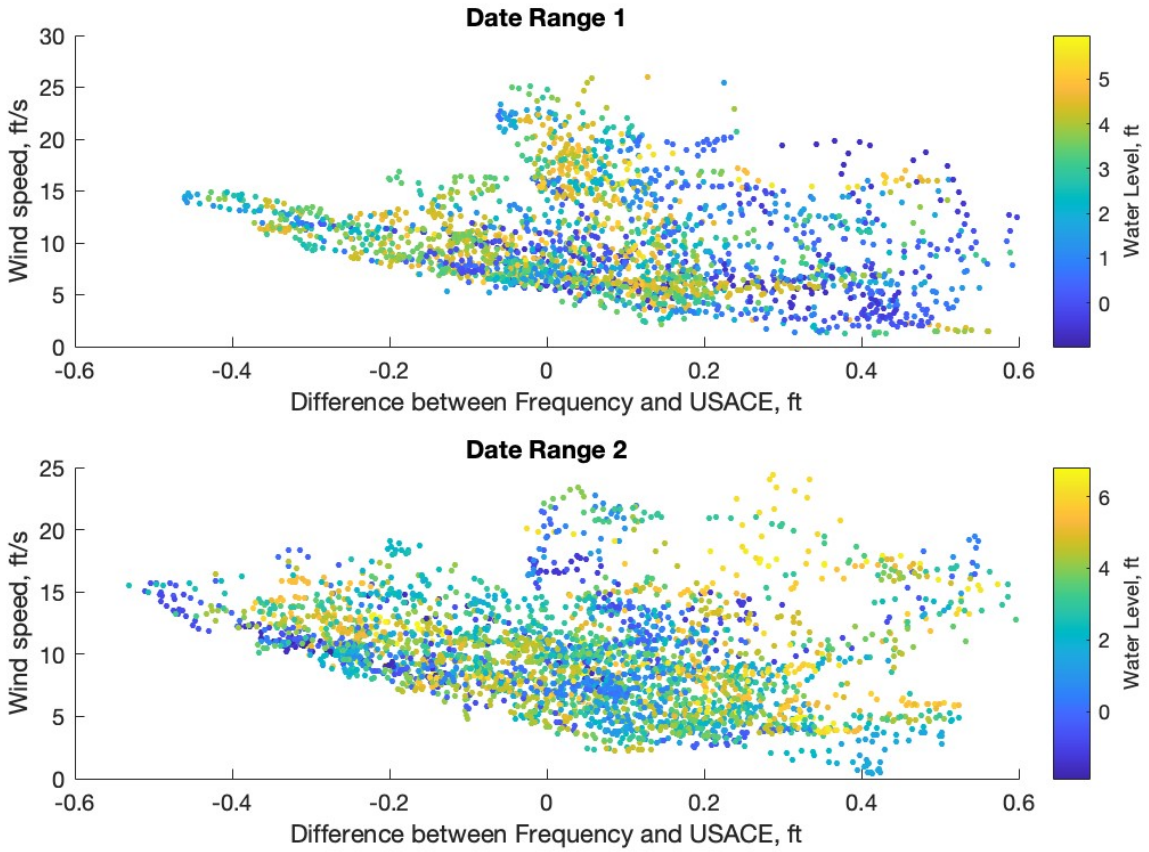

Figure 27b. Correlation between differences of Hs measurements and wind speed, water level. Color gradient represents water level. Date ranges separated by periods of viable wave gage data.

Similar to the comparison shown in Fig. 27a, low averaged wind speeds at lower water levels are typically under-predicted in the USACE equations in Date Range 1 as shown in Fig. 27b,

with higher water levels at higher wind speeds typically showing better agreement between the two methods. Higher water levels at higher wind speeds are conversely under-predicted by the USACE equations in Date Range 2 of Fig. 27b, and lower water levels more accurately or over-predicted by the USACE equations.

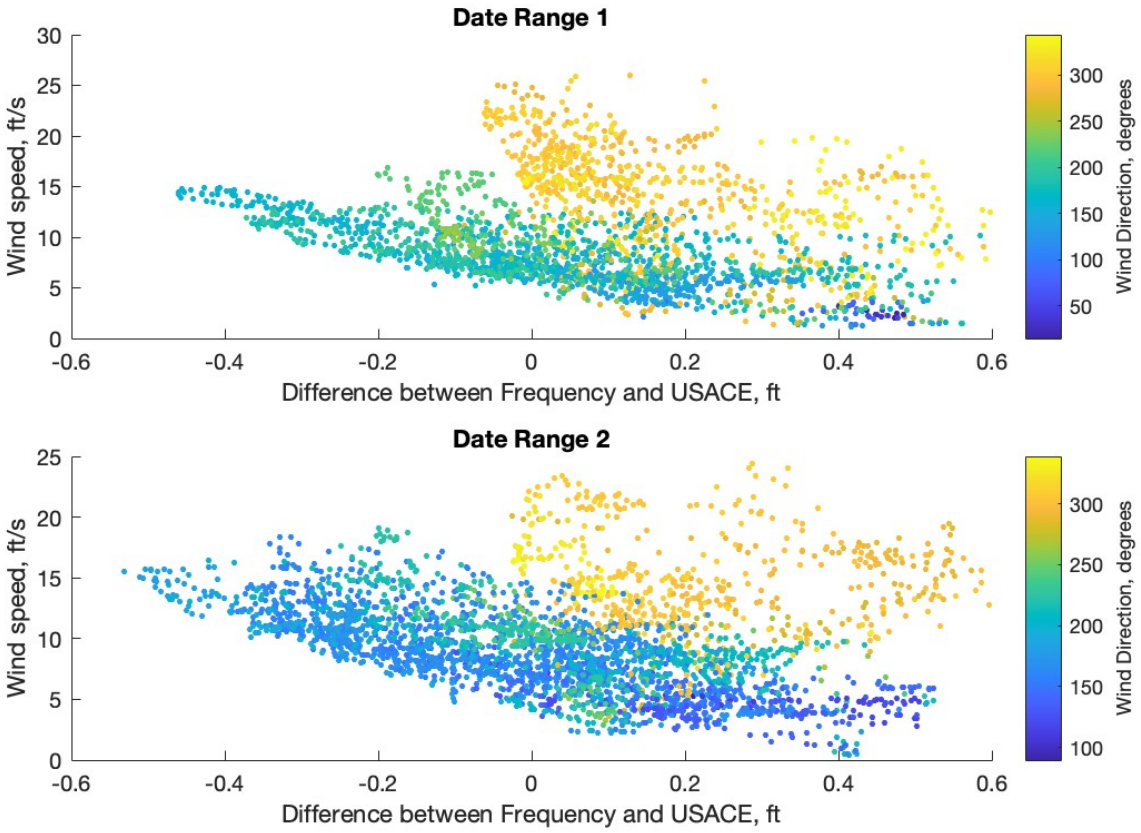

Figure 27c. Correlation between differences of Hs measurements and wind speed, wind direction. Color gradient represents wind direction. Date ranges separated by periods of viable wave gage data.

The comparison in Fig. 27c yields a clear trend in both date ranges. Higher degree (more northwesterly) winds tended to occur at higher wind speeds throughout the data collection period, and the USACE equations consistently under-predicted these values. Winds below

approx. 250 degrees, coming from the southwest, south, or southeast, were typically at lower speeds. The agreement between USACE and frequency wave height estimations here is more varied, although low-degree wind directions (<90 degrees) are also consistently under-predicted by the USACE equations, and an increasing wind speed tended to signify increasingly over-predicted wave heights.

A comparison of measured and theoretical wave period is shown in Figure 28.

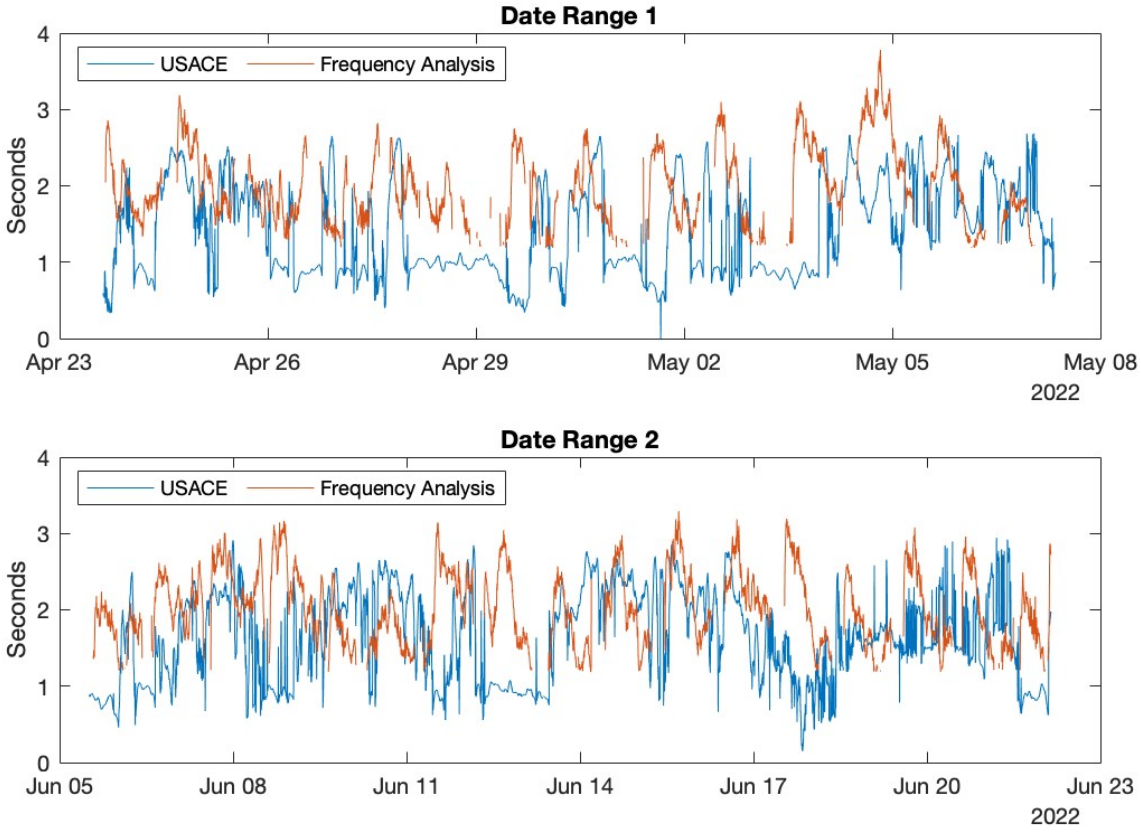

Figure 28. Comparison between measured and theoretical T values.

Date ranges separated by periods of viable wave gage data.

Like Fig. 26, periods calculated by USACE and frequency analysis methods share similar scales of magnitude, with T_{theory} ranging from 2.54 to 0 seconds at an average of 1.21 seconds and $T_{measured}$ ranging from 3.78 to 1.19 seconds at an average of 2.01 seconds. Also similar to Fig. 26, agreement between local maxima and minima in both date ranges don't share temporal agreement. Figures 29a-b display correlations between measured Hs and wind direction with wind speed and water level.

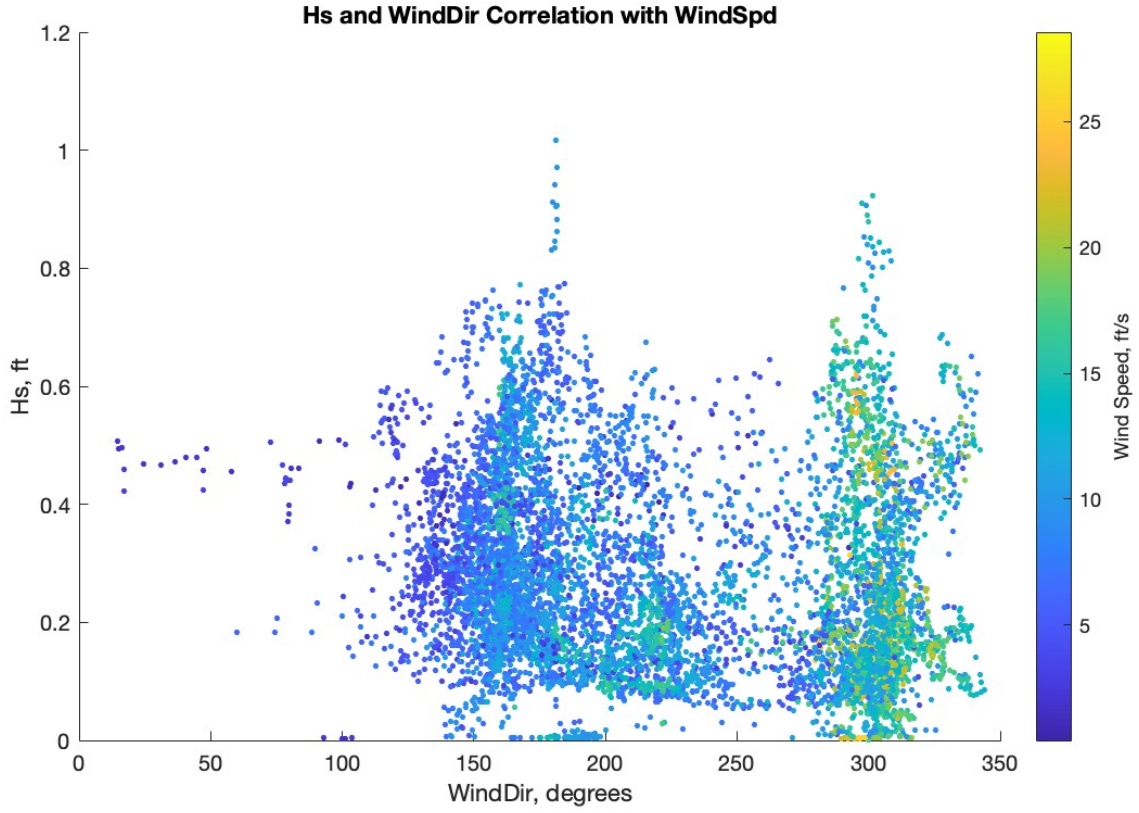

Figure 29a. Correlation between Hs_{meas} *and wind direction.*

Color gradient represents wind speed. Higher Hs_{meas} *values observed at 170 and 300 degrees. Stronger wind speeds primarily observed at 300 degrees (northwest winds).*

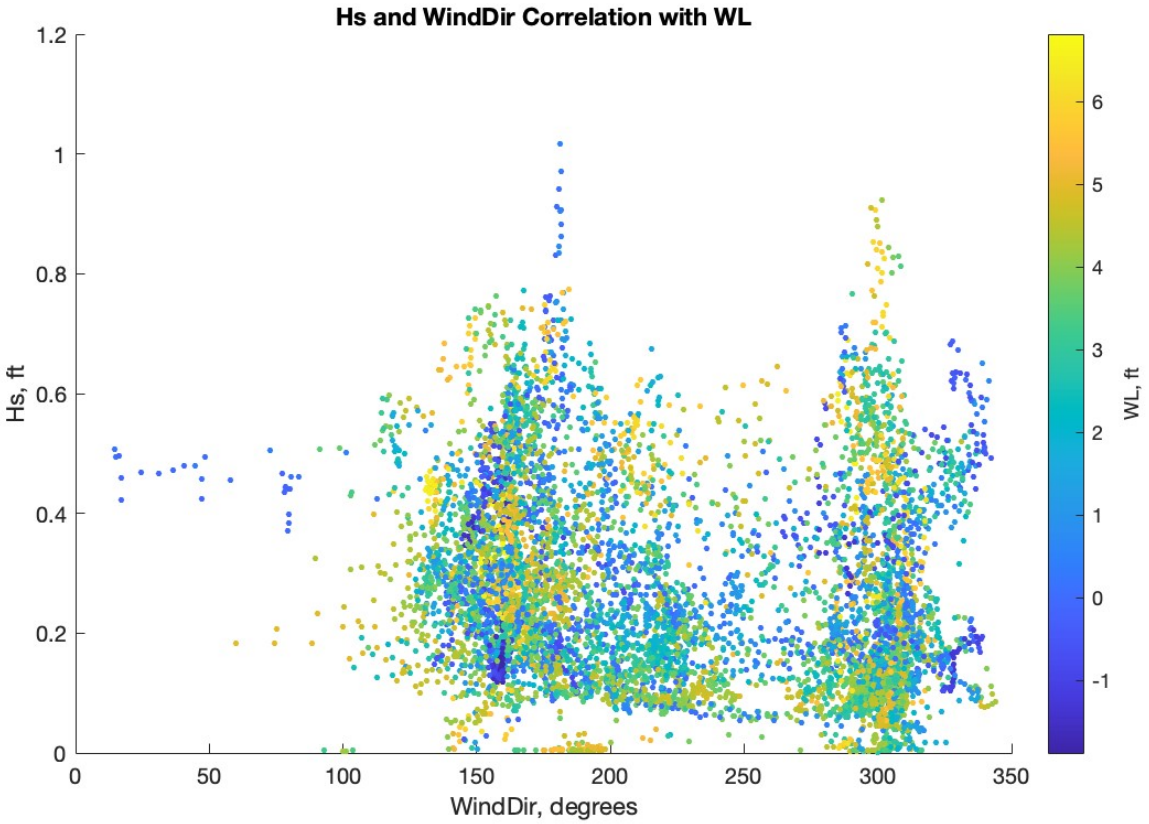

Figure 29b. Correlation between Hs_{meas} *and wind direction.*

Color gradient represents water level. Higher Hs_{meas} *values observed at 170 and 300 degrees.*

As Figures 29a-b show, while relatively high significant wave heights observable during the study period (>0.66 ft) were present during winds approaching from approximately 300 degrees, these conditions typically required higher water levels and faster winds to obtain similarly high wave heights observed during wind approach from 150-200 degrees.

d. TOPOGRAPHIC TRANSECTS

Results from the topographic surveys are shown in Figures 30a-d.

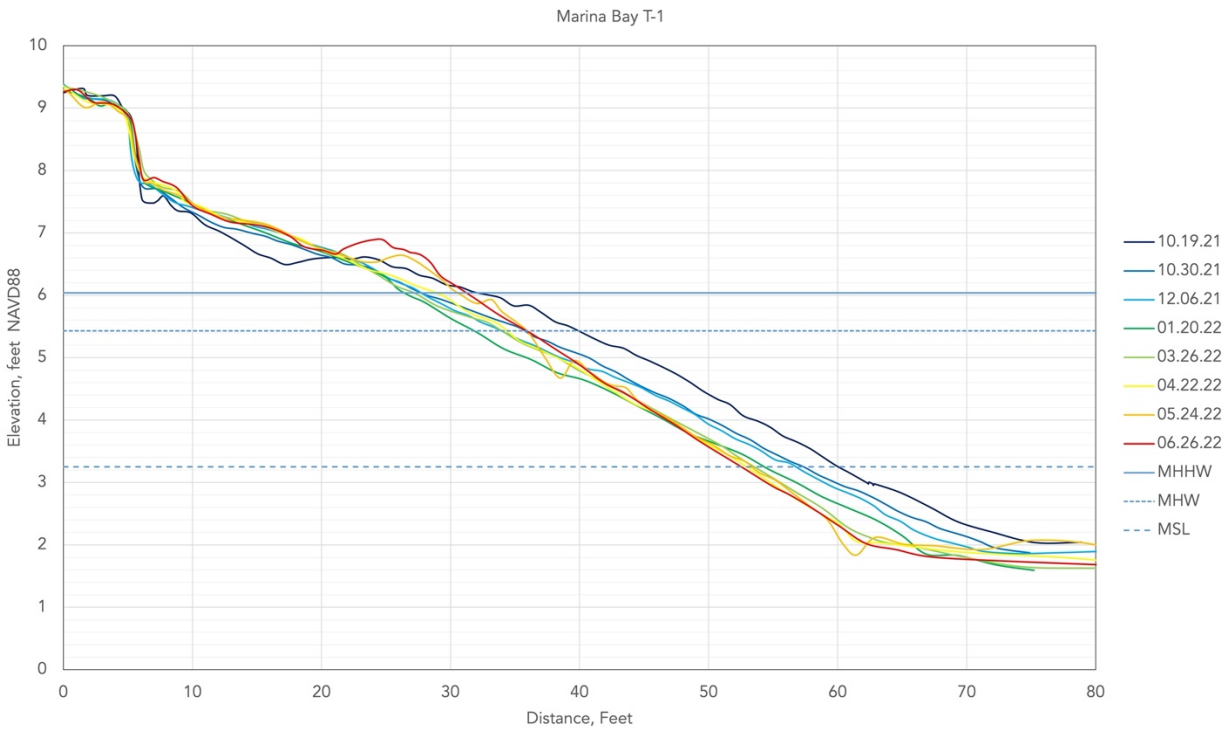

Figure 30a. T-1 topographic transect.

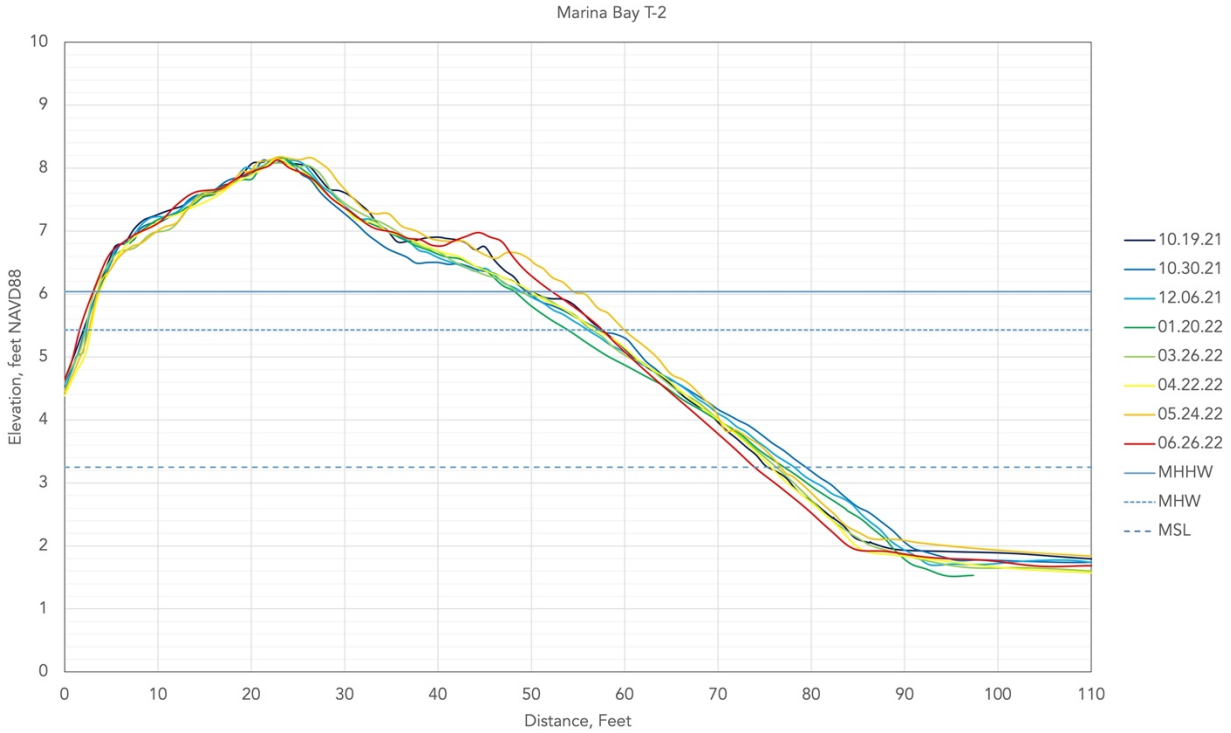

Figure 30b. T-2 topographic transect.

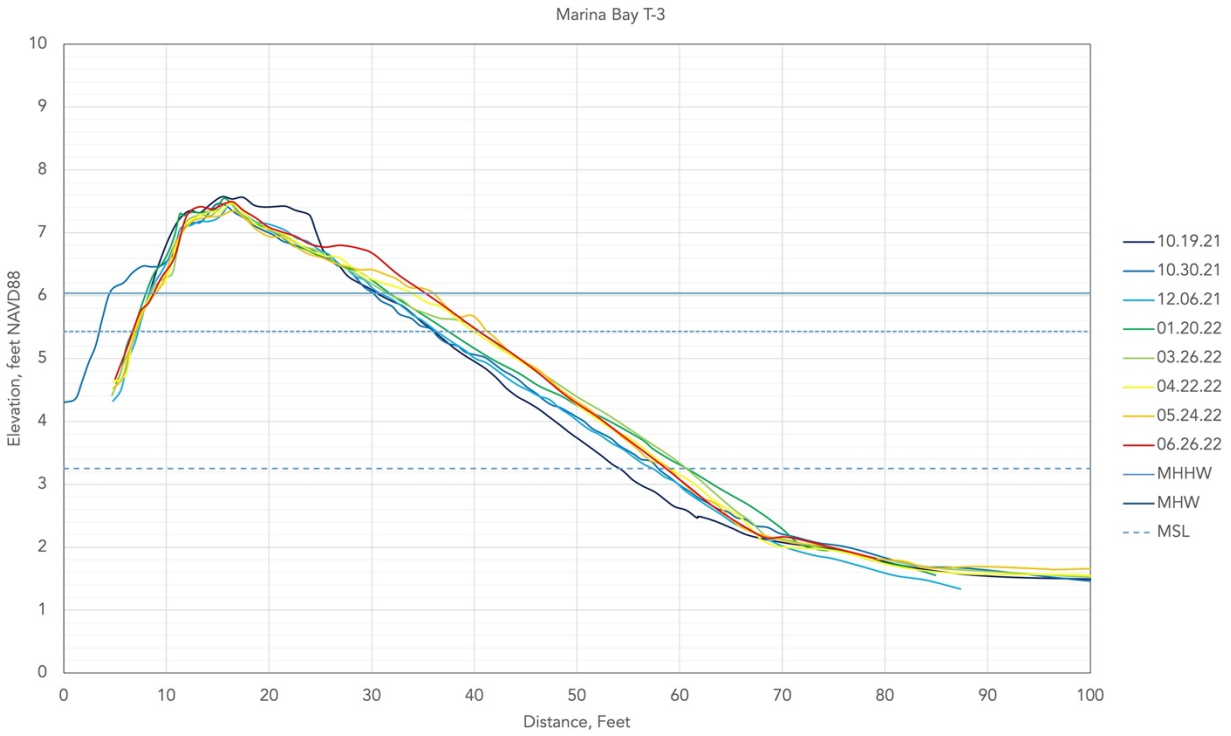

Figure 30c. T-3 topographic transect.

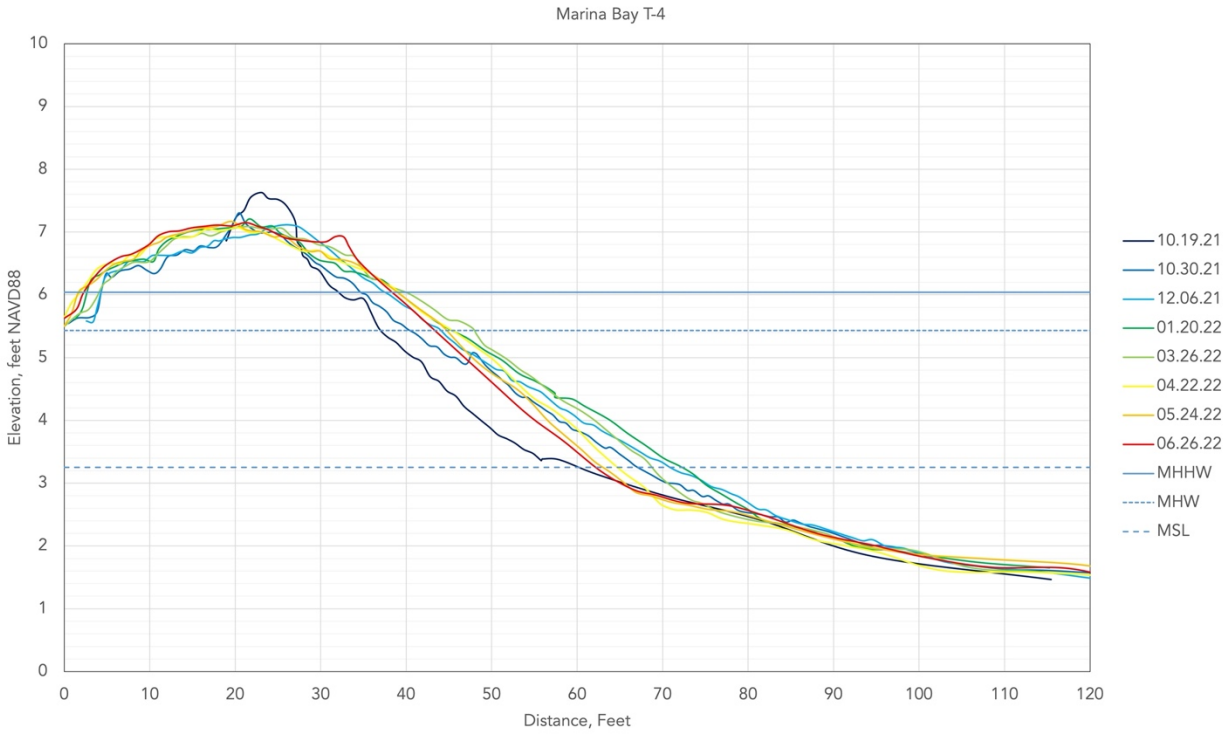

Figure 30d. T-4 topographic transect.

T-1 exhibits a marked flattening of the profile following the October 2021 storm event, with a 0.2′ decrease in profile in the lower beachface and a 0.2′ increase in the upper foreshore immediately beneath the shallow bluff. T-1 is the only site that exhibits a noticeable change in tidal flat elevation bayward of the beach toe; over the course of the survey period the tidal flat decreases by approximately 0.2′ in elevation. Also notable in the T-1 transect is the development of berm and runnel features during later summer months, on 24 May 2022 and 26 June 2022.

T-2 exhibited the least amount of incremental and overall profile change throughout the study period. The overall trend of a flattening profile following the 24 October 2021 storm event was similar to that of T-1, wherein the lower beachface experienced slight accretion and the upper beachface slight erosion. Profiles taken months later in the summer of 2022 display the formation of a bar that is widening and migrating upslope, approximating the original profile of 19 October 2021, and a lower beachface that is decreasing in elevation to a height similar to that of the 19 October 2021 date.

T-3 also experiences an overall post-storm flattening of the profile but contains a few notable differences from T-1 and T-2. For one, the washover deposits observed on 30 October 2021 are extended approx. 4′ further into the marsh, a section that isn't present during subsequent months. Additionally, the pre-storm berm is considerably wider (~12′) than in following survey events (~6′), unlike the relatively consistent crest width seen in T-2. Lastly, in the 2022 months,

the profile displays a similar 'recovery phase' to that of T-1 and T-2 and a beachface that remains elevated above the 19 October 2021 profile.

In T-4, the creation of the washover fan is seen. On 19 October 2021, the profile contains a crest located at approx. 7.6' elevation and clearly concave profile, with a small swash berm seen at +27' and a toe at +56'. The next survey date, 30 October 2021, shows a lowered crest at 7.25' and a convex profile, but most noticeably a washover fan that extends 20' behind the previous crest location and meets the marsh plain approximately 2' lower than the maximum beach elevation on 19 October 2021. In the following months, the lower beachface decreases in elevation and the toe location migrates back upslope, as the profile changes from convex to flat, with the formation of a relatively sizable swash bar present.

Beachface slope values are shown in Table 6. Slopes were calculated using points between MHHW and MSL. Excluding points above MHHW avoids irregular berm and overwash features, while excluding points below MSL avoids changes in slope associated with the beach toe and mudflat.

Table 6. Beach Slope

Date	T1	T2	T3	T4	Average
19 October 2021	0.10	0.11	0.14	0.12	0.12
30 October 2021	0.09	0.08	0.10	0.09	0.09
06 December 2021	0.10	0.10	0.10	0.08	0.10
20 January 2021	0.10	0.10	0.10	0.08	0.09
26 March 2022	0.11	0.10	0.10	0.10	0.10
22 April 2022	0.12	0.10	0.11	0.11	0.11
24 May 2022	0.12	0.13	0.12	0.12	0.12
26 June 2022	0.13	0.13	0.12	0.12	0.12
Average	0.11	0.10	0.11	0.10	0.11

The beach slope for the entire site, averaged over each transect at each date, is approximately 0.11, or a 1:9 slope. On 16 October 2021, all transects contain a slope that approximates the overall average for that location and display a gentler slope on 30 October 2021 following the October storm event. These transects also exhibit a gradual steepening of their slope in the following months. Ultimately, T-1 and T-2 contain a steeper slope on 26 June 2022 than on the initial survey event of 16 October 2021. The transects display a greater variability in slope on the initial survey date and much more similarity on the final survey date of 26 June 2022. Overall, the difference of average slopes between all transects is less than 0.01.

While not surveyed with the RTK equipment, one area of interest during site surveys was the eastern end of Marina Bay Beach, specifically at the transition between the Beach, the riprap embankment, and the marsh to the east. Figures 31 and A6a-f in Appendix A show this section of the site during the survey period.

Figure 31. Washover deposit at eastern end of Marina Bay Beach, 19 October 2021.

A shell and sand washover deposit could be seen on the marsh-side of the riprap, extending east and south as a recurve formation. Like the northern, cross-shore washover deposits, this washover form exhibited progressive exposure following storm events and covered vegetation following months of calmer conditions.

e. TRACER STUDY

Concentrations and centers of mass for each tracer survey event are shown in Table 7 and Figures A2a-e in Appendix A. A composite of all survey events conducted during the tracer experiment is shown in Figure 31. Transects taken at T-3 during tracer survey events, the profile on which the tracer was placed, is shown in Figure 33.

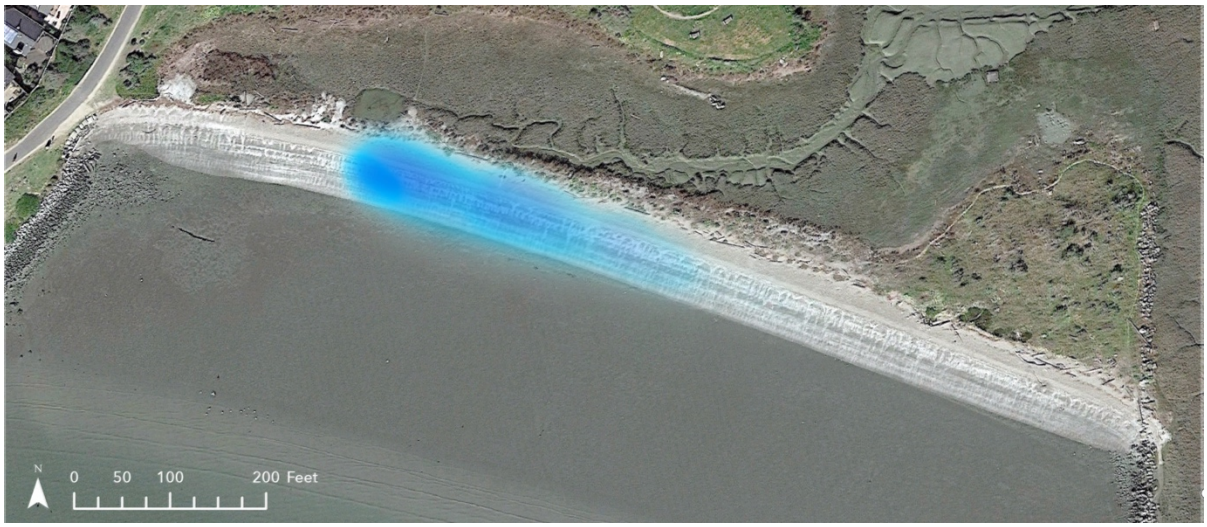

Figure 32. Tracer concentration composite.

Blue shading represents areas of detected tracer, overlaid from all five survey events. Darker shading represents a higher concentration of tracer.

Table 7. Tracer Development

Date	Ellipse Area (sf)	Center of Mass Distance from Origin (ft)
05/24/22	0	0.0
05/25/22	2780	14.7
05/26/22	2428	80.1
05/27/22	5718	112.3
05/28/22	6948	125.7
06/26/22	7276	180.3

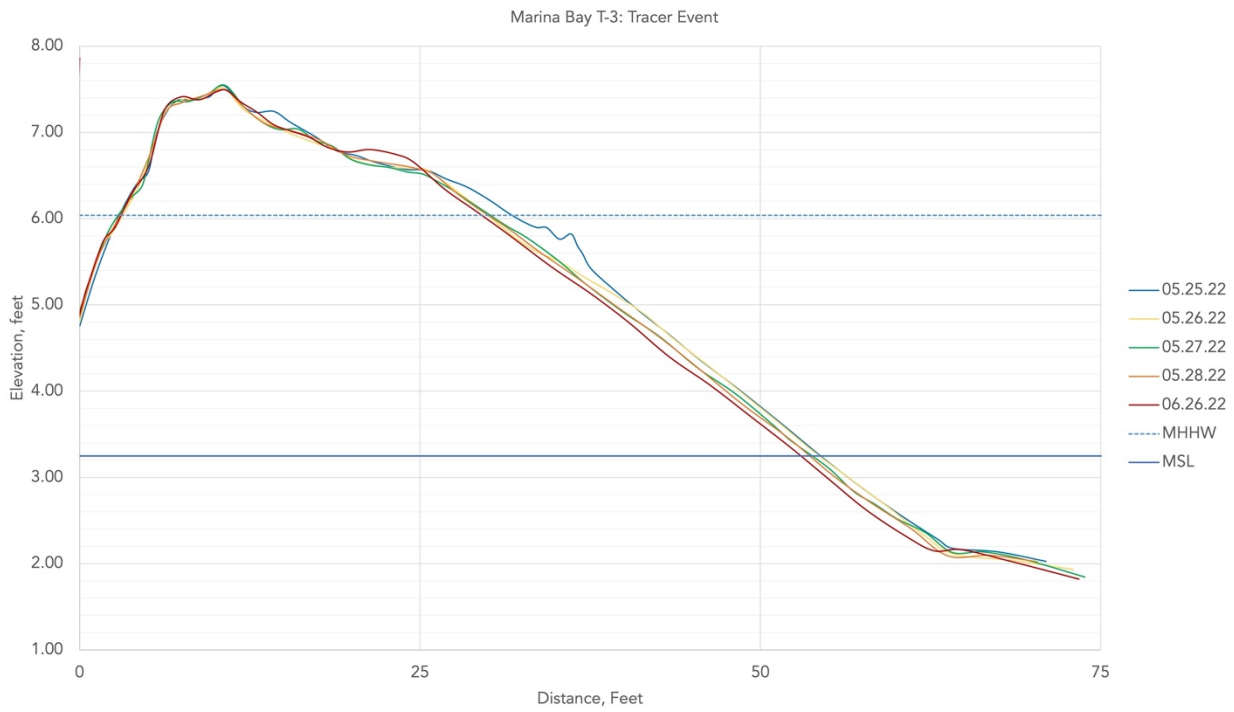

Figure 33. T-3 during tracer event.

Fig. 33 displays a transect that is largely stable throughout the deployment period, disregarding the upslope migration of the swash bar, matching the rising tides during this period. A slight lowering of the overall profile is also observable, which reinforces the finding of alongshore sediment transport observed in the tracer surveys.

As seen in Table 7, the greatest change in distance of center of mass occurred between 25 May 2022 and 26 May 2022 (65.4 ft), approximately 36 hours after initial deployment. The ellipse area represents one standard deviation of the spatial dispersion of the tracer. A greater ellipse area signifies a large spread of the tracer. Movement of the tracer was entirely eastward, with little to no grains present west of the deployment site. Little to no fluorescent sediment

was found on the dry berm, implying that negligible cross-shore aeolian transport took place during the study period.

Due to a malfunction in the pressure transducer, pressure data was not collected during this study period. Wind and water level conditions during the tracer study period from the NOAA Pt. Richmond station serve as approximations of wave conditions on the Beach (Figures 34a-b).

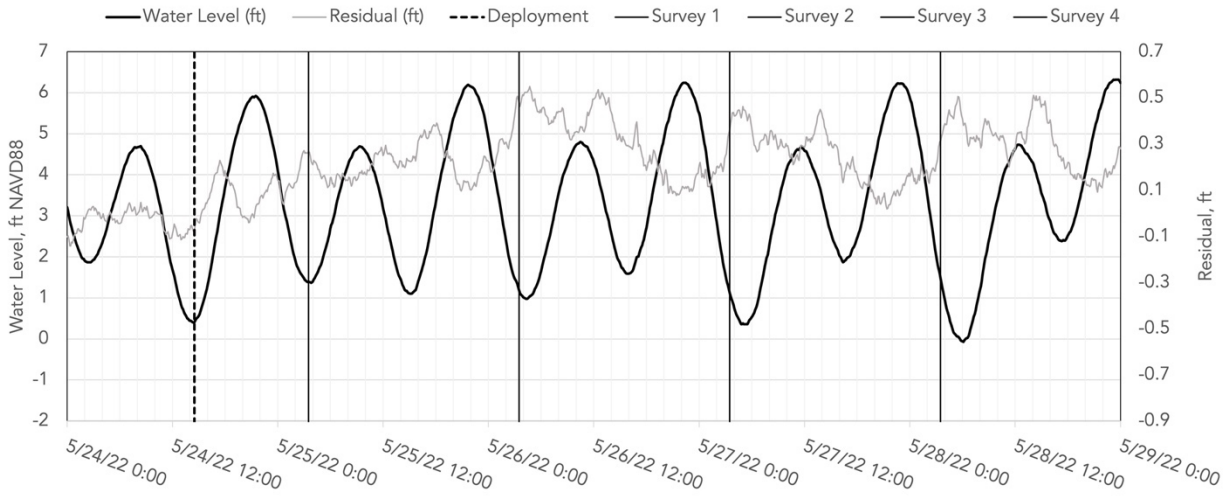

Figure 34a. Water level during tracer study, NOAA Pt. Richmond station.

Dark black line represents verified water level, gray line represents tidal residual. Dashed vertical line represents date of tracer deployment, solid vertical lines represent dates of subsequent tracer surveys.

Figure 34b. Wind conditions during tracer study, NOAA Pt. Richmond station.

Dark black line represents wind speed, gray dots represent wind direction. Dashed vertical line represents date of tracer deployment, solid vertical lines represent dates of subsequent tracer surveys.

The period of tracer study was during a neap tide. Water level and residual do not vary greatly, and winds largely remain under 20 ft/s. These conditions signify calm, summer-month conditions for the Beach.

f. GRAIN SIZE ANALYSIS

Full grain size analysis results are shown in Figure 35a-d, with D50 summaries shown in Table 8a-d.

Table 8a. T-1 D50 Results

Date	T-1 D50 (mm)				Avg (mm)*
16 October 2021	1.39	0.80	0.81	5.43	1.00
26 March 2022	0.40	1.24	1.58	0.10	0.83
26 June 2022	0.37	2.24	2.19		1.60
Average					1.22

Table 8b. T-2 D50 Results

Date	T-2 D50 (mm)				Avg (mm)*
16 October 2021	0.35	3.10	0.70	20.71	1.38
26 March 2022	0.35	2.30	1.11		1.25
26 June 2022	1.41	2.09	3.59		2.36
Average					1.67

Table 8c. T-3 D50 Results

Date	T-3 D50 (mm)				Avg (mm)*
16 October 2021	8.23	0.70	2.47	19.17	3.80
26 March 2022	0.38	1.26	0.43		0.69
26 June 2022	2.35	0.60	5.55		2.83
Average					2.44

Table 8d. T-4 D50 Results

Date	T-4 D50 (mm)				Avg (mm)*
16 October 2021	5.33	1.00	3.48	18.37	3.27
26 March 2022	1.34	5.35	0.33	3.03	2.51
26 June 2022	2.31	0.52	8.75		3.86
Average					3.16

**Note: Average D50 calculations exclude the fourth point sampled if present. These samples are located at lower intertidal mudflat, and typically contain fines with scattered cobble. These large cobble sizes and wide range in D50 values are not representative of the beachface sediment composition and are thus excluded from averages that are intended to be representative of beachface sediment.*

From D50 calculations, it can be shown that on average, the median sediment size for the Beach across all survey events is 2.12mm, corresponding to a sediment class of very fine gravel.

Figures 35a-d locate each sediment sample along the transect from where it was taken. While these locations are purposely not identical between survey events, they each identify the center of a zone of homogenous sediment type, e.g., sandy beach berm or medium gravel beach toe.

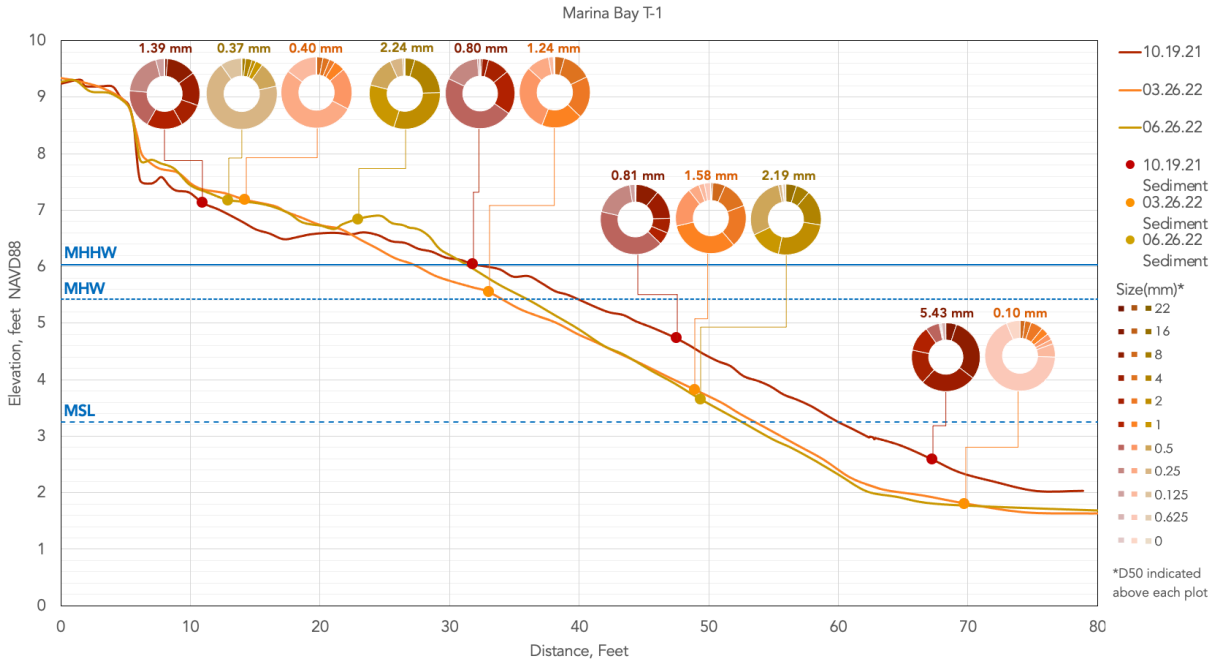

Figure 35a. T-1 grain size sample results.

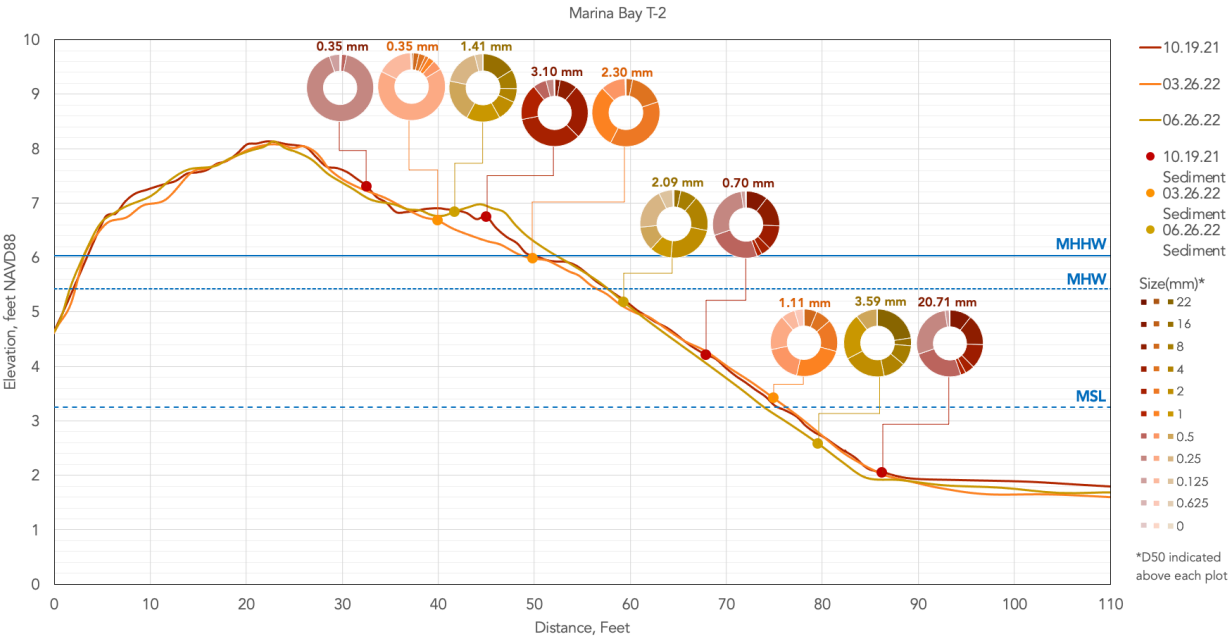

Figure 35b. T-2 grain size sample results.

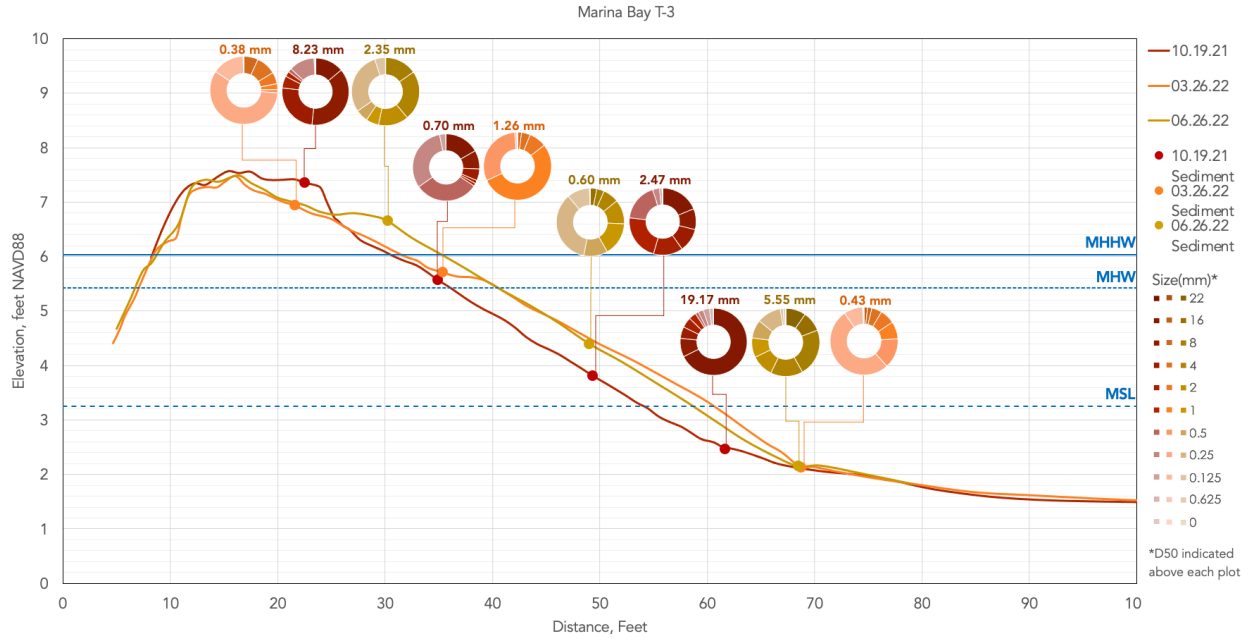

Figure 35c. T-3 grain size sample results.

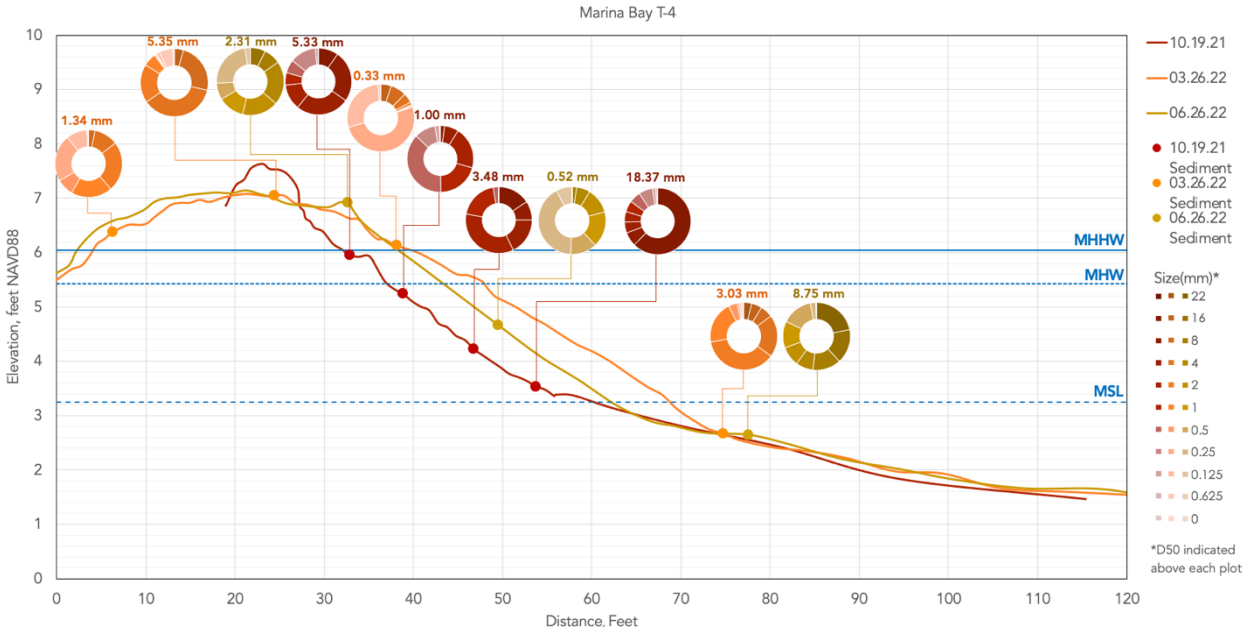

Figure 35d. T-4 grain size sample results.

Sediment results from T-1 bear several results when viewed in conjunction with the topographic profile. In the section directly beneath the bluff, the grain size becomes smaller, and the profile higher, following the 24 October 2021 storm event. This, along with field observations, implies that sandy sediment was eroded from and deposited at the base of the bluff, overlying coarser sediment at that location. The mid-beachface lowered considerably (~1 ft) after the initial survey event, with coarser samples than 19 October 2021, while the beach toe is similarly lowered but exhibits a much finer D50 than the initial sample.

T-2 contains samples on the upper beachface on 19 October 2021 and 26 March 2022 that share the same D50 of 0.35mm with a well sorted distribution, signifying a medium sand. A swash bar at or above MHHW was sampled on all three survey events, displaying a more poorly sorted distribution with a decreasing D50 size in successive events, from a 3.10mm and 2.30mm very fine gravel on 19 October 2021 and 26 Marsh 2022 respectively, to a 1.41mm very coarse sand on 26 June 2022. Also notable in this transect is the wide range in sediment sizes along the transect from the first survey event on 19 October 2021 to a narrower range during the following survey events.

The gravel berm seen on 19 October 2021 in T-3 is both absent in the topographic transect and in the sediment sample taken from 26 March 2022, which shows a fine sand D50. However, the swash bar evident on 26 June 2022 shows a coarser fraction at that location. Beachface samples at T-3 contain slightly differing D50 values between sample events, while samples at the toe show great variability between surveys.

The T-4 profile between 19 October 2021 and 26 March 2022 varied so considerably that direct comparison between the sediment samples on these dates is not straightforward. For instance, the beach toe moved out about +20 feet after 19 October 2021. The beach berm remained relatively coarse and poorly sorted throughout the study period but displayed a finer composition on 26 June 2022. Sampling of the washover fan on 26 March 2022 yielded a D50 of 1.34mm, equivalent to a very coarse sand, and contained a large proportion of shell.

In addition to the sample events, photos of pits excavated in the beachface and washover fans are qualitatively instructive in showing the vertical distribution of sediment, as shown in Figure A3 in Appendix A. Unlike beachface stratigraphy, which displayed scattered cobbles and a coarse basal layer at approx. 3 ft. NAVD88, the washover fan sampled close to T-3 exhibited a depth of roughly 30" (approx. 4.5 ft. NAVD88) and displayed well sorted sand and plant roots throughout the excavation pit.

VI. DISCUSSION

a. MORPHOLOGY

As observed in historical remote methods and field surveys, the hypothesis of decadal beach planform stability, disrupted by infrequent storm events, was confirmed. Washover deposits, transported cross-shore behind the Beach's berm, were evident in numerous historical aerial images and during a survey event in 2021. Evidence of less significant longshore transport was observed in topographic transects, a tracery survey, and grain size analysis.

i. Washover deposits

While not chronicled quantitatively, one factor influencing location and subsequent burial of washover fans at the Beach is site vegetation. Iceplant, wild fennel and other nonnative plants occupy sizable swaths of each end of Marina Bay Beach, where conglomerate substrate, heavy foot traffic and lack of inundation favors invasive species growth. In the central stretch of beach, washover deposits and backbarrier marsh however, several native species can be seen. Saltgrass and poverty weed were observed rapidly colonizing the washover fan observed at T-4, while beach saltbush and beach-bur, along with woody debris, helped stabilize the beach berm during storm events. In many locations, sediment was transported backshore to form a washover deposit between patches of established vegetation at the beach crest, and where vegetation or logs were present on the beach berm, sand-sized sediment was retained on the beachface. Plant roots found at varying depths throughout the washover fan excavation pit as seen in Fig. A3, signify successive cycles of calm wave conditions lacking backshore sediment

deposition and allowing plants to establish, followed by washover deposition, as identified in the aerial imagery.

It is also worth noting where along the beach the washover deposits were observed in the aerial imagery, as shown in Appendix Figures A1a-y. For most of the study period, washover deposits are present near T-3. However, the October 2021 storm yielded a rare instance of an overwash fan at T-4, the western-most edge of the site. This could be caused by the westward dominant wind direction during the storm event, changing vegetation patterns, or more transportable material exposed at this end of the beach that wasn't previously available.

While relatively small, the washover at the eastern end of the Beach as indicated in Fig. 31 highlighted the efficacy and shortcomings of the riprap edge as a sediment retention structure. While the embankment's presence likely retained larger volumes of sediment on the beach than were evident in the prevailing washover deposits, the retention structure's termination below MHHW allowed space for sediment to migrate over the riprap to the eastward marsh. The washover's elevation above MHHW and creation of a high tide refuge for shoreline birds was clear on the January 2022 king tide event, where birds preferred this stretch of beach to the adjacent riprap (see Fig. A6c). The clear accretion of fine gravel-sized sediment at this location in site photographs between 24 May 2022 and 26 June 2022 further reinforce the eastward-transport findings of the tracer study.

ii. Cross-shore transport and profile change

An overall comparison of the transects shows that T-2 contains the least amount of profile change following the initial survey date of 19 October 2021, whereas T-4 contains the most. This follows reason according to Nordstrom's theory of estuarine beach profile development, where profiles closest to the end of segments contain the most change, and those located within the middle, or antinode of segments contain less overall change (Nordstrom, 1992). Additionally, following a significant change between 19 October 2021 and 30 October 2021 for most profiles, each transect appears to display some degree of recovery in subsequent months, with the last survey date of 26 June 2022 often more closely approximating the pre-storm condition.

The October storm caused significant flattening of the beach profile, as material was pushed both landward and bayward, as evidenced by the formation of overwash fans and the expansion of the toe. Secondly, non-storm months from October 2021 to June 2022 exhibited a gradual steepening of the beach profile evident in the generally decreasing elevations of lower beachfaces and increasing elevations of upper beachfaces across transects, signifying a period of recovery and return to pre-storm conditions.

iii. Longshore transport

The immediate post-storm lowering of T-1, stability of T-2, slight raising of T-3 and considerable raising of T-4 imply a potential westward longshore transport direction during the

24 October 2021 storm event. This is reinforced by the dominant 150-degree wind direction of the storm shown in Fig 17b. This westward longshore movement observed during the October storm period is not seen during the study period of the tracer study, where a clear direction of eastward transport is present. The rate of tracer movement eastward accelerated between the first and second observation dates, which corresponds with wind increasing in speed and direction. The period of time between the second and third survey events continue to show southwestern winds, which justifies the continued eastward movement of the tracer. The overall rate of longshore transport during the tracer experiment exceeded expectations given water level and wind conditions during the first week of tracer deployment. This eastward direction of longshore transport is consistent with the grain size distribution across the site, which is typically coarser towards the western end. The westward longshore transport direction during the storm is perhaps indicative of southwesterly winds, which have a longer unobstructed fetch towards the beach site. Although more observation would be needed, these two findings suggest a quiescent eastward longshore transport at the Beach, interrupted by high-wind events approaching from the southwest that can cause morphological change.

iv. Waves

Within the collected dataset, it appears that the construction of a model that predicts actual wave height at the Beach given wind and water level data at the Pt. Richmond NOAA station is unattainable. The discrepancy between measured and theoretical values may decrease or become more identifiable with the collection of more data, particularly data during high wind

events. However, since the empirical USACE equations serve as rough approximations of nearshore wave parameters that are not universally applicable across sites, it is possible that convergence of the theoretical and measured data sets would not be achieved even with the collection of more data, and that the USACE equations are not applicable to the complex conditions present at this site within S.F. Bay. A few points are nonetheless notable from the USACE and measured wave height comparison. For one, waves are generated at the beach even when the wind direction is blowing off the beach, as seen in multiple figures. The historical wind direction and residual correlation from the NOAA Pt. Richmond station as seen in Fig. 20 is mostly consistent with the fetch map in Fig. 8 which neglects refraction, except that this data shows that there is a nontrivial possibility of residuals greater than 0.5 ft caused by winds approaching from the southwest (200-230 degrees) where the site is partially shielded by Brooks Island, and to a lesser extent from the northwest (290-330 degrees) where the site is entirely shielded by the Richmond shoreline. Figures 29a-b also suggest that strong northwest winds present during high tides, although approaching in a bayward direction relative to Marina Bay Beach, could create wave conditions throughout the Central Bay that are partially refracted and result in observable waves at the Beach. Figures 27a-c most clearly show how winds from these northwestern directions often contained higher relative speeds and measured wave heights were consistently under-predicted by the theoretical USACE equations. These findings imply that waves could be generated over the relatively long fetch in the North Bay and refracted around the Richmond headlands toward the beach. Whether these waves reach significant heights during storm conditions remains a question for future research.

b. METHODOLOGY

Integrated observations of Marina Bay Beach were gained through the application and analysis of several different field and remote data collection methods. However, each method has certain areas of improvement that could help inform future estuarine beach surveys.

i. Wave data

Measurements gained via pressure transducers were essential in understanding the wave climate at the site. The empirical equations for nearshore wave height from the USACE proved to be rough, insufficient approximations for an estuarine site's actual wave climate. It would be beneficial to collect more wave data from the site, particularly during months of stronger winds and specific storm events. Even collecting more data during calm conditions would help further refine the relationship between wind, water level and wave height at the study site, and deployment of an additional pressure transducers would aid in investigating some of the hypotheses behind direction of wave generation and tidal flat dissipation rates, particularly in regard to the possibly refracted waves originating in the North Bay. A more accurate theoretical comparison could be generated from hydrodynamic models such as SWAN wave model (Simulating WAves Nearshore) developed by TU Delft, which requires detailed inputs of bathymetry, currents, water levels, bottom friction, and wind (TU Delft, 2006). The assumption of no swell influence from the Golden Gate in the frequency analysis could also be tested, as WinklerPrins et al. (2021) and Rahbani et al. (2022) both showed evidence of partial swell influence in estuarine beach wave signatures.

Although the flow rate of tidal currents in the marsh behind the beach were not measured, whether these channels have the capacity to transport washover material away from the marsh is an interesting question for future research.

ii. Aerial imagery

While unsupervised classification on Google Earth imagery most reliably produced the most accurate results of subaerial beach area at the study site, additional classification methods could be tested using available satellite and aerial imagery. Shoreline position and subaerial beach area of other estuarine beaches in San Francisco Bay may be detectable by larger pixel-sized satellite imagery than was used in this study.

The historical comparison between water level, wind data and subaerial beach area could also be improved with more complete wind data or the selection of data subsets where all wind information is present. While elevated water levels can create conditions for morphological change to occur, onshore winds are still necessary to create high waves. Single storm events during one or several hours can create morphological change or washover deposits; this event could occur in a year when water levels did not often exceed MHHW. Thus, the probability represented by elevated water levels is not a direct corollary to the occurrence of storm events.

iii. Grain size analysis

Although the collection of grain samples, in conjunction with field and photo observations, can provide a representation of the beach's general sediment composition and prevailing characteristics throughout an eighth-month period, the infrequency of sampling did not allow for the analysis of event-scale surface movement dynamics. For future studies it is recommended that grain size sampling be conducted during an initial survey to establish modal sediment characteristics, and at specific, closely spaced intervals corresponding to pre- and post-storm conditions thereafter. Additionally, field notes should have been taken to document lateral changes in sediment composition, as opposed to relying only on samples withdrawn from areas of homogenous sediment composition. Also, sample locations could have been standardized between events, i.e., designating that one sample always be extracted from the beach berm, middle beachface, beach toe and mudflat.

While qualitatively more stable and coarser than other mudflats around the Bay, additional samples taken from the mudflat at Marina Bay Beach would have aided in comparison of this site to others throughout the Bay. Analyzing samples from the backbarrier marsh would also help identify whether a coarse sediment fraction from washover events has noticeably entered the marsh substrate.

iv. Tracer study

In general, dyed sediment remained most visible at the high tide swash bar just below the beach berm and at the beach toe. Dyed sediment was not visible within the lower intertidal mudflat, although was presumably present there given its visibility at the beach toe. At the end of the tracer observation on 26 June 2022, dye was noticeably fading from shell and gravel, although remained visible on smaller sand particles. The tracer study did not contain analysis of the tracer's movement with depth in the beach and was not able to register fluorescent sediment within the mudflat. As with the wave data collection, results would conceivably improve with additional observations of the tracer's movement. Surveying multiple transects during the study period, instead of a single one, would also help confirm the direction and magnitude of longshore transport.

c. FUTURE PROJECTIONS

Marina Bay Beach is an interesting hybrid of a shoreline: it was created by an anthropogenic fill, but naturally reworked by waves into a beach that experiences a wider range of natural dynamics than other man-made beaches in the Bay. It is constrained on both ends of by riprap embankments, which shelter it from most directions of incoming wave approach, similar to naturally occurring headland-bound, bluff-backed pocket beaches in the North Bay. However, it intergrades with a backbarrier marsh, similar to marsh-fringing barrier beaches of the southern Central Bay. This combination may be responsible for the relatively unique occurrence of overwash fans present at the site. Unlike drift-aligned marsh-fringing beaches

where strong wave action transports sediment alongshore, strong wave action at Marina Bay Beach results in cross-shore transport during storm events. And unlike other swash-aligned beaches where cross-shore sediment exchange is often constrained by a bluff, sediment at Marina Bay Beach can be transported over the crest of the Beach.

Marina Bay Beach also differs from previously identified contexts of washover deposits in San Francisco Bay, where typically thin layers of sediment are deposited on marsh plains. At those sites, the beach crest is typically only slightly higher than the marsh. At Marina Bay, the beach crest is several feet higher than the marsh. This difference in elevation could alter the form in which washover is deposited behind the beach. Instead of thin layers that are pushed further back along the marsh plain during overwash events, sediment at Marina Bay Beach falls directly behind the crest, and is able to accrete vertically with successive washover deposits. While not investigated in this study, this dynamic could have led from an historically sharp, levee-like transition between beach and marsh to the development of a landward-sloping backshore, transitioning more gradually in sediment composition and vegetation from a tidal marsh to a beach berm. Thus, the beach has conceivably served both as a protective wave barrier and a transition slope to the backbarrier marsh. However, after this initial, single pulse of wave-reworked construction debris sediment, the beach's only source of sediment appears to be infrequent erosion of the adjacent path to its western end, and the artificial bluff to its eastern end.

With continued storm events that carry sediment over the beach crest at a rate that exceeds sediment replenishment, it is possible that sand-sized sediment will be depleted from the present beachface and intergrade further into the marsh through washover fans, creating a hillocky, heterogeneous topography that will create different zones of marsh vegetation. A coarse lag deposit could remain in its present location on the western end of the beach as finer sediment continues to erode, creating the foundation for a gently sloping intertidal terrace as sea levels rise, creating an inlet into the backbarrier marsh during high tides. Due to the presence of the conglomerate upland area on the backshore of the eastern end of the Beach, further washover and transgression of the beach at this location is unlikely.

The marsh behind the Beach faces similar threats to its existence. If sediment deposition at this location does not keep pace with sea-level rise, the Bay Trail currently behind the marsh will be at the water's edge during high tide in a few decades. During storms, waves could eventually overtop the Bay Trail if not effectively buffered by the newly submerged marsh and beach. Against the steeper barrier of the Bay Trail embankment, wave energy will be reflected, increasing stress on the remaining bayward marsh and beach. Nourishment of Marina Bay Beach should be considered as a management opportunity to protect the marsh and backbarrier Bay Trail. To maintain crest elevations and avoid erosion that lowers the beach crest as was observed at T-4, beach crest vegetation and woody debris could be used to prevent localized washover deposits, as they proved effective at the Beach during the October 2021 storm event.

VII. CONCLUSION

This study attempts to contribute to the ongoing work of research, restoration, and creation of estuarine beaches in San Francisco Bay in two regards. For one, the description and relative success of various remote and field study methodologies may serve as useful for those looking to refine these methods and study other sites within the Bay. Secondly, the identification of historic and contemporary overwash fans highlights a mechanism of beach transgression that should be fully considered in BEB nourishment projects.

With the exception of these periodic, high-wind event-driven events of cross-shore sediment exchange, Marina Bay Beach has generally exhibited long-term stability in planform, in part due to its artificially embayed setting. However, transects, grain size analysis, a tracer study and field observations confirmed longshore transport during high-wind and quiescent conditions. Waves approaching from the south / southeast historically exhibited the highest water level set up at the study site, although measured wave data identified northwesterly winds as a potential source for wave generation at the site, despite its sheltered location from the North Bay.

As a significant sediment source does not appear to naturally feed the site, it seems plausible that future strong wave events will continue to create washover deposits at the Beach, further pushing back the profile and creating low points within the crest where overwash can occur more frequently.

In general, study of estuarine beaches may require several spatiotemporal scales of analysis. Coarse, decadal scale methods including historic wind and water level analysis, and aerial imagery analysis provide useful for overall observations on beach morphology. The findings of topographic transects, field observations and wave data may be most applicable on an annual scale, building up incremental datasets that display clearer findings over several years rather than several seasons. Methods including tracer deployment and grain size analysis could have the most practicality during episodic events, tracking the hourly or daily evolution of the beach in response to particular wave conditions. As the governing characteristics of these landscapes are varied and interdependent, future research should strive for a holistic approach to estuarine beach observation and analysis.

VIII. REFERENCES

Atwater, B.F. 1979. Ancient processes at the site of southern San Francisco Bay: movement of the crust and changes in sea level, in San Francisco Bay: the urbanized estuary, T.J. Conomos (ed), Pacific Division, American Association for the Advancement of Science, San Francisco, California.

Barad, K. 2021. Personal communication.

Barnard, P.L, Schoellhamer, D.H., Jaffe, B.E. and McKee, L.J. 2013. Sediment transport in the San Francisco Bay Coastal System: An overview. Marine Geology. 345: 3-17.

Battalio, B. 2014. Littoral processes along the Pacific and bay shores of San Francisco, California, USA. Shore & Beach, 82(1).

Bishop, C.T. and Donelan, M.A. 1987. Measuring waves with pressure transducers. Coastal Engineering, 11: 309-328.

Bracewell, J. 2017. Establishment of benchmarks, transects, and geodatabases—Version 1.0. Gulf Coast Network standard operating procedure NPS/GULN/SOP—CT02. Gulf Coast Network, Lafayette, Louisiana.

Bunte, K. and Abt, S.R. 2001. Sampling surface and subsurface particle-size distributions in wadable gravel- and cobble-bed streams for analyses in sediment transport, hydraulics, and streambed monitoring. United States Department of Agriculture, General Technical Report RMRS-GTR-74.

San Francisco Bay Area Water Trail (BAWT), 2020. Site Description for Crane Cove Park.

Baye, P. 2021. Personal communication.

Baye P. and Leventhal R. 2020. Conceptual designs for sea level rise adaptation: Greenwood and Brunini Beaches, Tiburon, Richardson Bay, Marin County, California. Task 3 Report for "New Life for Eroding Shorelines", San Francisco State University – Estuary & Ocean Science Center, Tiburon California. Prepare for California State Coastal Conservancy.

Baye, P., Leventhal, R., and Beagle, J. 2020. Conceptual designs for marsh-fringing beach nourishment to reduce wave erosion of Muzzi Marsh, Corte Madera Ecological Reserve, Marin County, California. Task 3 technical memorandum for "New life for eroding shorelines." Prepared for California State Coastal Conservancy, Oakland California.

Beagle J.R., Salomon M., Baumgarten S.A., Grossinger R.M. 2015. Shifting shores: Marsh expansion and retreat in San Pablo Bay. Prepared for the US EPA San Francisco Bay Program and the San Francisco Estuary Partnership. Publication #751, San Francisco Estuary Institute, Richmond, CA.

Cleary, W.J., Hosier, P.E., and Wells, G.R. 1979. Genesis and significance of marsh islands within southeastern North Carolina lagoons. Journal of Sedimentary Petrology (49)3: 0703-0710.

Coastal Engineering Research Center, Department of the Army, Waterways Experiment Station, Corps of Engineers (USACE). 1984. Shore Protection Manual. Volume I, Fourth Edition.
Cooper J.A.G., Lewis D.A. and Pilkey O.H. 2007. Fetch-limited barrier islands: Overlooked coastal landforms. GSA today 17(3): 4-9. doi: 10.1130/GSAT01703A.1.

Conomos, T.J. 1979. Properties and circulation of San Francisco Bay waters, in San Francisco Bay: the urbanized estuary. Pacific Division, American Association for the Advancement of Science, San Francisco, California.

DeWeerdt, S. 2022. 'Invertebrate engineers' combat sea level rise. Encyclopedia of Puget Sound, Salish Sea Currents Magazine. https://www.eopugetsound.org/magazine/living-dike-shoreline-protection

East Bay Regional Park District (EBRPD). 2013. Crown Memorial State Beach sand replacement fact sheet.

Crosby, S.C., Sax, D.F., Palmer, M.E., Booth, H.S., Deegan, L.A., Bertness, M.D., and Leslie, H.M. 2016. Salt marsh persistence is threatened by predicted sea-level rise. Estuarine, Coastal and Shelf Science 181: 93-99. doi: 10.1016/j.ecss.2016.08.018

Elsey-Quirk, T., Mariotti, G., Valentine, K., and Raper, K. 2019. Retreating marsh shoreline creates hotspots of high-marsh plant diversity. Scientific Reports (9)5795. doi: 10.1038/s41598-019-42119-8

Fellowes, T.E., Vila-Concejo, A., Gallop, S.L., Schosberg, R., de Staercke, V., and Largier, J.L. 2021. Decadal shoreline erosion and recovery of beaches in modified and natural estuaries. Gemorphology, 390. https://doi.org/10.1016/j.geomorph.2021.107884

Gallop, S.L., Vila-Concejo, A., Fellowes, T.E., Harley, M.D., Rahbani, M., and Largier, J.L. 2020. Wave direction shift triggered severe erosion of beaches in estuaries and bays with limited post-storm recovery. Earth Surface Processes and Landforms, 45, 3854-3868.

Goodfellow, B.W., and Stephenson, W.J. 2014. Beach morphodynamics in a strong-wind bay: a low-energy environment? Marine Geology, 214: 101-116. doi: 10.1016/j.margeo.2004.10.022

Grossinger, R.M., Askevold, R.A., and Collins, J.N. 2005. T-Sheet user guide. Application of the historical U.S. Coast Survey Maps to environmental management in the San Francisco Bay Area. San Francisco Estuary Institute (SFEI), Report No. 427.

Jackson N.L., Nordstrom K.F., Eliot, I., and Masselink G. 2002. 'Low energy' sandy beaches in marine and estuarine environments: a review. Geomorphology 48, p. 147-162.

Kinsman, N., and Xu, J.P., 2012. Fluorescent tracer experiment on Holiday Beach near Mugu Canyon: U.S. Geological Survey Open-File Report 2012-1131. (Available at http://pubs.usgs.gov/of/2012/1131/.)

Lacy, J.R. and MacVean, L.J. 2016. Wave attenuation in the shallows of San Francisco Bay. Coastal Engineering 114: 159-168. doi: 10.1016/j.coastaleng.2016.03.008

Leventhal, R. and Baye, P. 2021. Beaches as an alternative to riprap and walls for eroding shorelines. Sierra Club SLR Symposium.

Lorang, M.S. and Stanford, J.A. 1993. Variability of shoreline erosion and accretion within a beach compartment of Flathead Lake, Montana. Limnol. Oceanogr. 38(8): 1783-1795.

Maurmeyer, E.M. 1978. Geomorphology and evolution of transgressive estuarine washover barriers along the western shore of Delaware Bay.

Morton, R.A., and A.H. Sallenger Jr.. 2003. Morphological impacts on extreme storms on sandy beaches and barriers. Journal of Coastal Research. 19(3): 560-573.

National Oceanic and Atmospheric Administration (NOAA). 2016. NOAA historical surveys (T-Sheets). NOAA shoreline website, https://shoreline.noaa.gov/data/datasheets/t-sheets.html

National Oceanic and Atmospheric Administration (NOAA). 2022. Richmond, CA – Station ID: 9414863. https://tidesandcurrents.noaa.gov/stationhome.html?id=9414863

NOAA, SAGE and USACE. 2015. Natural and structural measures for shoreline stabilization.
Nordstrom, K.F. 1980. Cyclic and seasonal beach response: A comparison of oceanside and bayside beaches. Physical Geography, 1(2): 177-196. doi: 10.1080/02723646.1980.10642199

National Park Service (NPS). 2020. World War II shipbuilding in the San Francisco Bay Area. https://www.nps.gov/articles/000/world-war-ii-shipbuilding-in-the-san-francisco-bay-area.htm

Nordstrom, K.F. 1992. Estuarine beaches: An introduction to the physical and human factors affecting use and management of beaches in estuarine, lagoons, bays and fjords. Springer Netherlands. ISBN: 9781851667284.

Nordstrom K.F., and Jackson N.L. 2012. Physical processes and landforms on beaches in short fetch environments in estuaries, small lakes and reservoirs: A review. Earth-Science Reviews 111, p. 232-247. doi: 10.1016/j.earscirev.2011.12.004

Petek, G. 2020. What threat does sea-level rise pose to California? Legislative Analyst's Office.

Pilkey, O.H. 2011. The world's beaches. University of California Press. ISBN 9780520268722.

Philip Williams & Associates, Ltd. And Treadwell & Rollo (PWA). 2009. Coyote Point Recreation Area phase 2 – preliminary design report. Prepared for San Mateo County Parks Department. PWA Ref.1876.02.

Rahbani, M., Vila-Concejo, A., Fellowes, T.E., Gallop, S.L., WinklerPrins, L., and Largier, J.L. 2022. Spatial patterns in wave signatures on beaches in estuaries and bays. Gemorphology, 398. https://doi.org/10.1016/j.geomorph.2021.108070

Rosie the Riveter / World War II Home Front National Historical Park (NPS). 2010. Richmond Marina Bay Trail. National Park Service, U.S. Department of the Interior, Richmond California.

San Francisco Bay Restoration Authority (SFBRA), 2020. Heron's Head Park shoreline resilience project: Phase 1. Staff Recommendation. Project No. RA-017, Project Manager Marilyn Latta.

SCAPE, 2020. Coarse grain beach webinar. Hosted by California Coastal Conservancy, Exploratorium, and University of California, Davis.

Schoellhamer, D. H., 2011. Sudden clearing of estuarine waters upon crossing the threshold from transport- to supply-regulation of sediment transport as an erodible sediment pool is depleted: San Francisco Bay, 1999. Estuaries and Coasts, 34: 885–899.

SFEI and Baye, P. 2020. New life for eroding shorelines: Beach and marsh edge change in the San Francisco Estuary. Publication #984, Version 1.0, San Francisco Estuary Institute, Richmond, CA.

SFEI and SPUR. 2019. San Francisco Bay Shoreline Adaptation Atlas: Working with Nature to Plan for Sea Level Rise Using Operational Landscape Units. Publication #915, San Francisco Estuary Institute, Richmond, CA.

South Richmond Shoreline Special Area Plan Citizen's Advisory Committee (SAP). 1987. South Richmond Shoreline Special Area Plan. An Amendment to the City of Richmond General Plan and the San Francisco Bay Conservation and Development Commission Bay Plan.

Toure, S., Diop, O., Kpalma, K., and Maiga, A.S. 2019. Shoreline detection using optical remote sensing: A review. International Journal of Geo-Information 8(75). doi: 10.3390/ijgi8020075

TU Delft (Delft University of Technology). 2006. SWAN User Manual. The SWAN team, TU Delft, Faculty of Civil Engineering and Geosciences, Environmental Fluid Mechanics Section.

United States Geologic Survey (USGS) and Dingler, J. 1994. Coastal wetlands and sediments of the San Francisco Bay system. doi:10.3133/25156

University of California, Berkeley (UCB). 2005. Richmond Field Station marsh remediation and restoration.
https://web.archive.org/web/20070816033632/http://www.cp.berkeley.edu/RFS_MarshRR.html

Vila-Concejo, A., Gallop, S.L., and Largier, J.L. 2020. Sandy beaches in estuaries and bays. Sandy Beach Morphodynamics, 343-362. http://dx.doi.org/10.1016/B978-0-08-102927-5.00015-1

Vos, K., Splinter, K.D., Harley, M.D., Simmons, J.A., and Turner, I.L. 2019. CoastSat: A Google Earth Engine-enabled Python toolkit to extract shorelines from publicly available satellite imagery. Environmental Modelling and Software 122. doi: 10.1016/j.envsoft.2019.104528

Wentworth C.K. 1922. A scale of grade and class terms for clastic sediments. Journal of Geology, 30(5): 377-392. doi10.1086/622910.

Wetlands and Water Resources, Inc. (WWR), Leventhal R., and Baye P. 2010. Aramburu Island shoreline protection and ecological enhancement project draft enhancement plan. Prepared for Richardson Bay Audubon Sanctuary.

WinklerPrins, L., Largier, J.L., Vila-Concejo, A., Gallop, S.L., Rellowes, T.E., and Rahbani, M. 2021. Components and tidal modulation of the wave field in a semi-enclosed shallow bay. Earth ArXiv, preprint. doi: 10.31223/X5P612

APPENDIX A. ADDITIONAL FIGURES

Table A1 below represents the inventory of beaches referred to in Figure 2. Beaches are listed starting from the Golden Gate in San Francisco and continue counterclockwise around the Bay.

Table A1. Inventory of distinct San Francisco Bay beaches.

	Beach Name	Jurisdiction
1	Chrissy Field Beach	San Francisco
2	Coghlan Beach	San Francisco
3	Aquatic Park Beach	San Francisco
4	Clipper Cover Beach	San Francisco
5	Yerba Buena Island Beach 1*	San Francisco
6	Yerba Buena Island Beach 2*	San Francisco
7	Yerba Buena Island Beach 3*	San Francisco
8	Crane Cove Park Beach	San Francisco
9	Pier 94 Beach	San Francisco
10	India Basin Beach	San Francisco
11	Heron's Head Beach	San Francisco
12	Oyster Point Beach	South San Francisco
13	Aardvark Beach	San Mateo
14	Coyote Point Beach	San Mateo
15	San Mateo Beach*	San Mateo
16	Foster City Beach 1*	Foster City
17	Foster City Beach 2*	Foster City
18	Foster City Beach 3*	Foster City
19	Belmont Slough Beach	Foster City
20	Erckenbrack Park Beach	Foster City
21	Gull Park Beach	Foster City
22	Marlin Park Beach	Redwood City
23	Bird Island Beach	Redwood City
24	Bair Island Beach 1*	Redwood City
25	Bair Island Beach 2*	Redwood City
26	Russell Beach	San Leandro
27	Long Beach	San Leandro
28	Alameda Beach	Alameda
29	Crown Memorial State Beach	Alameda
30	Encinal Beach	Alameda
31	Encinal Cove Beach*	Alameda
32	Middle Harbor Shoreline Beach	Oakland
33	Bay Bridge Beach*	Oakland
34	Radio Beach	Oakland
35	Toll Plaza Beach	Oakland
36	Emeryville Marsh Beach	Oakland
37	Point Emery Beach	Emeryville
38	Barkley Beach	Berkeley
39	South Sailing Basin Beach*	Berkeley
40	Berkeley Marina Beach*	Berkeley
41	Schoolhouse Creek Beach*	Berkeley
42	Fleming Point Beach	Albany
43	TEPCO Beach	Richmond
44	Point Isabel Beach*	Richmond
45	Marina Bay Beach	Richmond
46	Brooks Island Beach 1*	Richmond
47	Brooks Island Beach 2*	Richmond
48	Keller Beach	Richmond
49	Point Molate Beach	Richmond
50	Point Orient Beach 1*	Richmond
51	Point Orient Beach 2*	Richmond
52	Point San Pablo Beach 1*	Richmond
53	Point San Pablo Beach 2*	Richmond
54	Point San Pablo Beach 3*	Richmond
55	Point San Pablo Beach 4*	Richmond
56	Point Pinole Beach 1*	Richmond
57	Point Pinole Beach 2*	Richmond
58	Point Pinole Beach 3*	Richmond

	Beach Name	Jurisdiction
59	Giant Marsh Beach 1*	Richmond
60	Giant Marsh Beach 2*	Richmond
61	Garrity Creek Beach 1*	Richmond
62	Garrity Creek Beach 2*	Bayview-Montalvin
63	Wilson Point Beach 1*	Bayview-Montalvin
64	Wilson Point Beach 2*	Bayview-Montalvin
65	Pinole Bayfront Park Beach	Pinole
66	Pinole WWTP Beach*	Pinole
67	Pinole Creek Beach*	Pinole
68	Hercules Headland Beach*	Hercules
69	Lone Tree Point Beach	Rodeo
70	Rodeo Sanitary District Beach 1*	Rodeo
71	Rodeo Sanitary District Beach 2*	Rodeo
72	Eckley Pier Beach*	Crockett
73	Dillon Point Beach 1*	Vallejo
74	Dillon Point Beach 2*	Vallejo
75	Glen Cove Waterfront Park Beach	Vallejo
76	Carquinez Heights Beach*	Vallejo
77	Vallejo Beach 1*	Vallejo
78	Vallejo Beach 2*	Vallejo
79	Mare Island Beach*	Vallejo
80	Glass Beach	Sonoma
81	Gallinas Creek Beach	Santa Venetia
82	Rat Rock Cove Beach	Santa Venetia
83	China Camp Beach	San Rafael
84	Dillingham Beach	San Rafael
85	McNears Beach	San Rafael
86	Point San Pedro Beach*	San Rafael
87	Pogy Point Beach*	San Rafael

	Beach Name	Jurisdiction
88	Brickyard Beach 2*	San Rafael
89	Brickyard Beach	San Rafael
90	San Rafael Creek Beach*	San Rafael
91	Starkweather Shoreline Park Beach	San Rafael
92	San Quentin Beach 1*	San Quentin
93	San Quentin Beach 2*	San Quentin
94	San Quentin Beach 3*	San Quentin
95	Paradise Cay Beach*	Tiburon
96	El Campo Beach 1*	El Campo
97	El Campo Beach 2*	El Campo
98	Paradise Cove Beach*	El Campo
99	Point Chauncey Beach*	El Campo
100	Bluff Point Beach	El Campo
101	Tiburon Linear Park Beach	Tiburon
102	Blackie's Pasture Beach	Tiburon
103	Sanctuary Beach	Tiburon
104	Strawberry Beach*	Strawberry
105	Aramburu Island Beach	Strawberry
106	Schoonmaker Beach	Sausalito
107	Swede's Beach	Sausalito
108	Perles Beach	Tiburon
109	Sand Springs Beach	Tiburon
110	Quarry Beach	Tiburon
111	Angel Island Beach 1*	Tiburon
112	Angel Island Beach 2*	Tiburon
113	Angel Island Beach 3*	Tiburon
114	Angel Island Beach 4*	Tiburon
115	Angel Island Beach 5*	Tiburon
116	Yellow Bluff Beach*	Mill Valley
117	Horseshoe Cove Beach*	Mill Valley

** indicates beaches for which no official name could be found. For the purposes of this inventory, beaches were named for prominent geologic features or landmarks.*

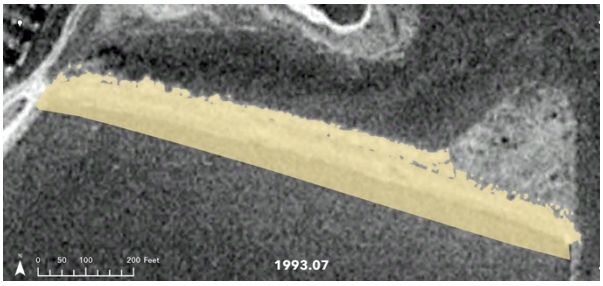

Figure A1a. Subaerial beach area 1993.07.

Figure A1b. Subaerial Area 2002.10

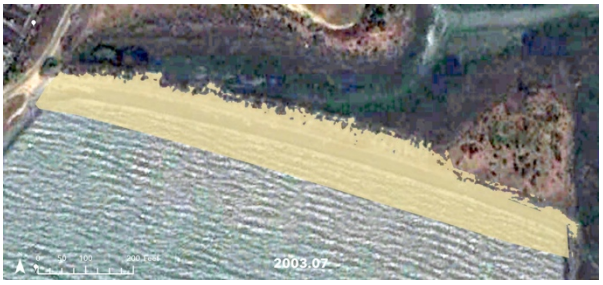

Figure A1c. Subaerial Area 2003.07

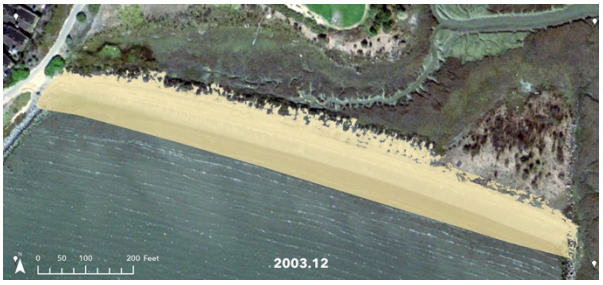

Figure A1d. Subaerial Area 2003.12

Figure A1e. Subaerial Area 2004.09

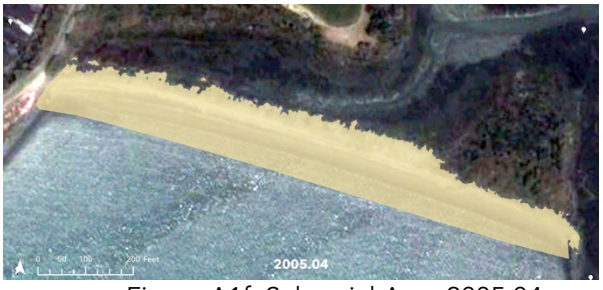

Figure A1f. Subaerial Area 2005.04

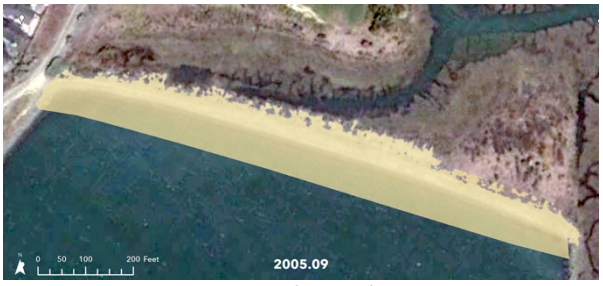

Figure A1g. Subaerial Area 2005.09

Figure A1h. Subaerial Area 2007.05

Figure A1i. Subaerial Area 2007.06

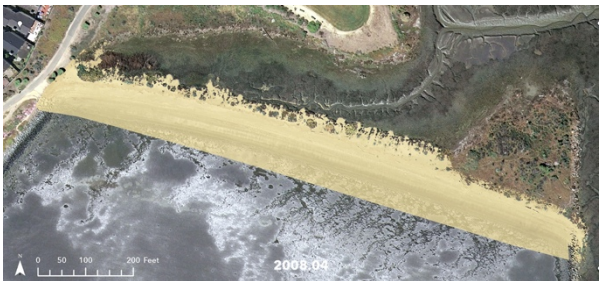

Figure A1j. Subaerial Area 2008.04

Figure A1k. Subaerial Area 2009.10

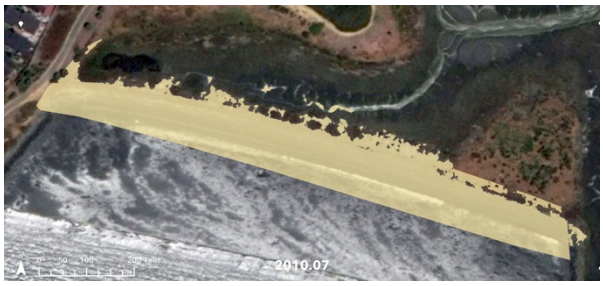

Figure A1l. Subaerial Area 2010.07

Figure A1m. Subaerial Area 2011.10

Figure A1n. Subaerial Area 2012.08

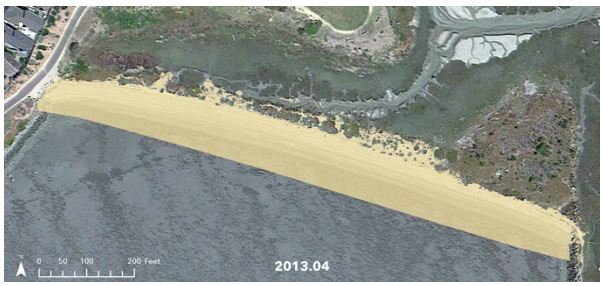

Figure A1o. Subaerial Area 2013.04

Figure A1p. Subaerial Area 2014.03

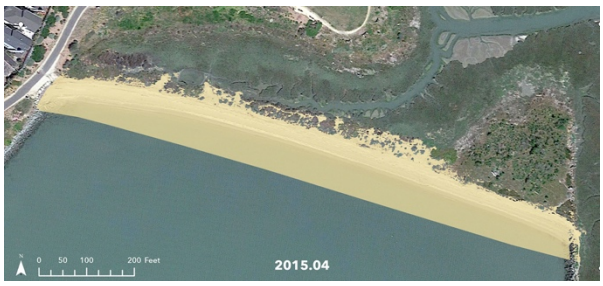

Figure A1q. Subaerial Area 2015.04

Figure A1r. Subaerial Area 2016.03

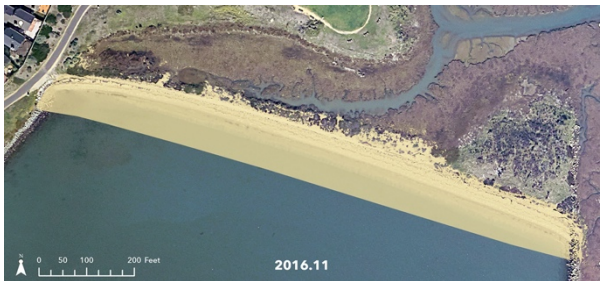

Figure A1s. Subaerial Area 2016.11

Figure A1t. Subaerial Area 2017.03

Figure A1u. Subaerial Area 2018.03

Figure A1v. Subaerial Area 2019.06

Figure A1w. Subaerial Area 2020.08

Figure A1x. Subaerial Area 2021.02

Figure A1y. Subaerial Area 2022.02

Figure A2a. Tracer 25 May 2022

Figure A2b. Tracer 26 May 2022

Figure A2c. Tracer 27 May 2022

Figure A2d. Tracer 28 May 2022

Figure A2e. Tracer 26 June 2022


Figure A3. Overwash Fan Pit, 20 January 2022

Overwash at T-3, Looking West

Fig A4a. T-3 Backshore, 19 October 2021

Fig A4b. T-3 Backshore, 30 October 2021

Overwash at T-3, Looking East

Fig A5a. T-3 Backshore, 19 October 2021

Fig A5b. T-3 Backshore, 30 October 2021

Fig A5c. T-3 Backshore, 30 November 2021

Fig A5d. T-3 Backshore, 5 December 2021

Fig A5e. T-3 Backshore, 06 December 2021

Fig A5f. T-3 Backshore, 20 January 2022

Fig A5g. T-3 Backshore, 22 April 2022

Fig A5h. T-3 Backshore, 26 June 2022

Overwash at Eastern End

Fig A6a. Eastern End, 19 October 2021

Fig A6b. Eastern End, 30 October 2021

Fig A6c. Eastern End, 02 January 2022

Fig A6d. Eastern End, 20 January 2022

Fig A6e. Eastern End, 22 April 2022

Fig A6f. Eastern End, 26 June 2022

Overwash at T-4, Looking West

Fig A7a. T-4 Backshore, 19 October 2022

Fig A7b. T-4 Backshore, 30 October 2021

Fig A7c. T-4 Backshore, 5 December 2021

Fig A7d. T-4 Backshore, 06 December 2021

Fig A7e. T-4 Backshore, 02 January 2022

Fig A7f. T-4 Backshore, 26 March 2022

Fig A7g. T-4 Backshore, 22 April 2022

Fig A7h. T-4 Backshore, 26 June 2022